JOURNAL OF GEOPHYSICAL RESEARCH, VOL. 103, NO. B12, PAGES 29,759–29,779, DECEMBER 10, 1998

The size distribution of pyroclasts and the fragmentation sequence in explosive volcanic eruptions

E. Kaminski and C. Jaupart

Laboratoire de Dynamique des Systèmes Géologiques, Institut de Physique du Globe de Paris

Abstract. In an explosive eruption, the atmospheric column dynamics depend strongly on the mass fraction of gas in the erupting mixture, which is fixed by fragmentation in the volcanic conduit. At fragmentation, gas present in vesicular magmatic liquid gets partitioned between a continuous phase separating magma clasts and a dispersed phase in individual bubbles within the clasts. As regards flow behavior, it is the former, continuous, gas phase which matters, and we show that its amount is determined by the fragment size. Analysis of 25 fall deposits and 37 flow deposits demonstrates that ash and pumice populations follow a power law size distribution such that N, the number of fragments with radii larger than r, is given by $N \propto r^{-D}$. D values range from 2.9 to 3.9 and are always larger than 3.0 in fall deposits. D values for pyroclastic flow deposits are systematically smaller than those of fall deposits. We show that at fragmentation the amount of continuous gas phase is an increasing function of the D value. Large D values cannot be attributed to a single fragmentation event and are due to secondary fragmentation processes. Laboratory experiments on bubbly magma and on solid pumice samples demonstrate that primary breakup leads to D values of 2.5 ± 0.1 and that repeated fragment collisions act to increase the D value. A model for size-dependent refragmentation accounts for the observations. We propose that in a volcanic conduit, fragmentation proceeds as a sequence of events. Primary breakup releases a small amount of gas and is followed by fragment collisions. Due to refragmentation and decompression, both the mass and volume fractions of continuous gas increase. The final D value, and hence the mass fraction of continuous gas at the vent, depends on the time spent between primary fragmentation and eruption out of the vent.

1. Introduction

Explosive volcanic eruptions eject a large mass of magma fragments, ranging from meter-sized blocks to micron-sized ash particles dispersed at high altitudes in the atmosphere. This population of fragments is the end result of processes operating in the volcanic conduit and in the atmosphere (Figure 1). A key process is "fragmentation," such that bubbly magma disintegrates into fragments [*Wilson*, 1976; *Sparks*, 1978]. In most eruption models, this is taken to occur when the volume fraction of gas bubbles in vesicular magma exceeds a threshold value, which is usually taken to be 75% [*Sparks et al.*, 1994; *Woods*, 1995]. Such a threshold criterion is appealing because of its simplicity but obscures several important questions regarding the mixture of gas and fragments which is generated. For example, neither the sizes of the fragments nor the interactions between the two components of the mixture get specified. In physical models of the eruption process, fragmentation is also taken to mark a change of flow dynamics, from a laminar regime involving viscous and vesicular magma to a turbulent regime involving a mixture of gas and suspended fragments. Thus the term "fragmentation" amalgamates two different and important changes: a topological change for the gas and liquid phases and a change of dynamics.

As regards magma, fragmentation essentially marks a transition from a continuous to a dispersed phase. As regards the exsolved gas, the situation is more complicated because gas gets partitioned in two different phases: a continuous phase which separates the magma fragments, and a second phase of bubbles within the fragments. In a fragment, only those bubbles which are connected to the surface are able to leak gas to the continuous phase. The dispersed gas phase plays no active role and basically acts to lower the density of fragments with respect to pure magma. For the flow regime, it is the continuous gas phase which matters most, because it carries the magma fragments in suspension and because it controls flow behavior in the atmosphere. Determining the respective proportions of the two gas phases is therefore critical. One may envisage two end-member situations. In one limit, each and

Paper number 98JB02795.
0148-0227/98/98JB-02795$09.00

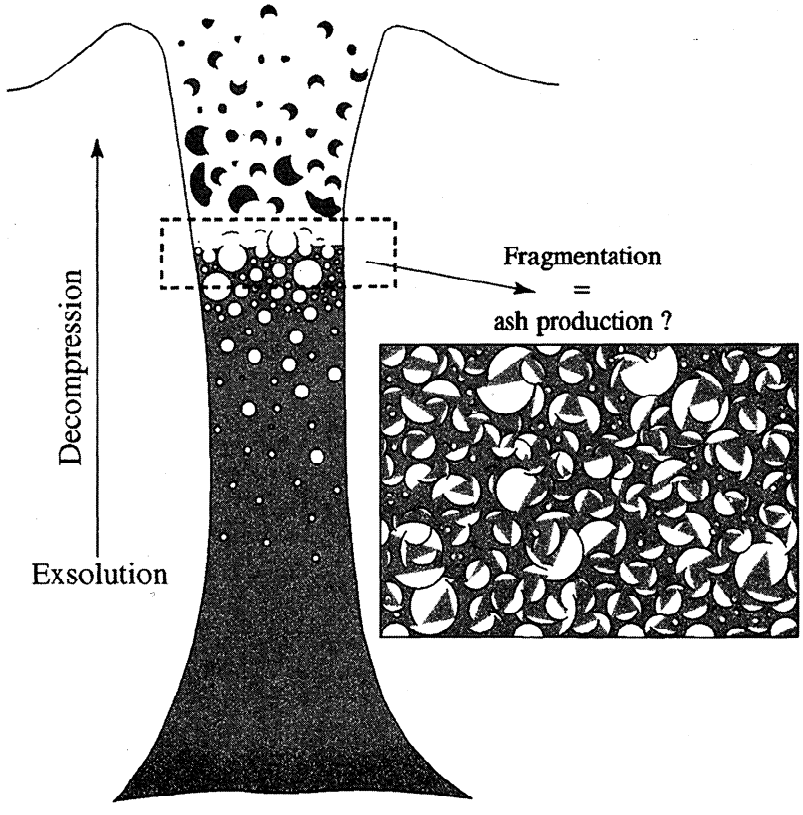

Figure 1. Schematic representation of the main processes occurring in an eruptive conduit. At fragmentation, bubbly magma breaks up into a number of fragments. A common assumption is that all the gas present collects into a continuous phase carrying the fragments. This implies that only ash particles are generated by fragmentation, which is not consistent with the presence of pumice samples in pyroclastic deposits.

every gas bubble gets disrupted and all magma fragments are vesicle free. We shall call this the "complete atomization limit," such that all the exsolved gas collects into a continuous phase (Figure 1). In the other limit, the magma fragments are large and retain a large number of bubbles inside. In this case, the continuous gas phase is a tortuous network separating the fragments, and the mixture of gas and fragments does not behave as a suspension. Pumice samples from pyroclastic deposits are highly vesicular and provide evidence for gas kept within fragments [*Gardner et al.*, 1996; *Kaminski and Jaupart*, 1997] (Appendix A), suggesting that the "complete atomization" limit may not be a valid approximation.

The above argument implies that the mass fraction of continuous gas in the volcanic mixture depends on fragmentation. Thus fragmentation not only separates between "explosive" and "effusive" eruption regimes but may also determine which explosive regime ensues. Consider, for example, the Plinian and pyroclastic flow regimes. In the Plinian case, the erupted material becomes lighter than surrounding air and a buoyant column develops to high altitudes in the atmosphere. In the pyroclastic flow regime, the eruption column collapses at some height above the vent [*Sparks and Wilson*, 1976; *Woods*, 1995]. Specifying which regime prevails requires knowledge of the mass fraction of gas at the vent, which involves three steps. The first step is to estimate the amount of volatiles dissolved in the melt at depth [*Rutherford et al.*, 1985; *Anderson et al.*, 1989]. The second step is to predict how bubbles nucleate and expand due to pressure release and to specify the mechanism of fragmentation. This has been the focus of much recent research, involving field studies [*Houghton and Wilson*, 1989; *Klug and Cashman*, 1994; *Gardner et al.*, 1996], theoretical calculations [*Valentine and Wohletz*, 1989; *Proussevitch et al.*, 1993; *Maccdonio et al.*, 1994; *Woods*, 1995] and laboratory experiments [*Anilkumar et al.*, 1993; *Mader et al.*, 1994; *Sugioka and Bursik*, 1995; *Lyakhovsky et al.*, 1996; *Alibidirov and Dingwell*, 1996]. The third step is to specify how much gas gets released during and after fragmentation. Up until now, this third step has been overlooked and calculations have been made in the "complete atomization" limit [e.g., *Woods*, 1995]. As will be demonstrated here, this leads to an upper bound on the amount of continuous gas in the volcanic mixture. Our major goal in this paper is to evaluate how far from this limit true volcanic mixtures are.

Understanding how fragmentation proceeds and what

fragment sizes are generated is important for realistic flow models [*Wilson et al.*, 1980; *Woods and Bursik*, 1991]. Fragments typically account for more than 90% of the volcanic mixture mass, and hence carry the mass, momentum, and energy fluxes of the flow. The dynamical interactions between gas and fragments depend critically on size, and large fragments can achieve large thermal anomalies and differential velocities with respect to surrounding gas. Most published models do not account for this, notable exceptions being those by *Woods and Bursik* [1991] and *Neri and Macedonio* [1996], and it is important to evaluate the resulting errors.

In this paper, we use published data on the sizes of magma fragments from a large number of Plinian and pyroclastic flow deposits. We show that these fragment populations follow a power law size distribution with very specific values of the exponent, and we discuss how this provides constraints on the fragmentation process itself as well as on the dynamics of explosive volcanic eruptions. From a broader perspective, pumice and ash populations offer a striking example of fragmented materials encompassing a very large range of sizes (typically more than 4 orders of magnitude). The field data, laboratory experiments, and analysis given in this paper have implications for fragmentation mechanisms in general [e.g., *Redner*, 1990].

2. Amount of Gas Released at Fragmentation

Fragmentation leads to the formation of individual bubble-bearing magma fragments. For the following argument, this process may be represented as fractures, or interfaces, developing through bubbly magma. Bubbles intersected by these fractures release their gas, in contrast to bubbles buried deeply in the fragments which can only leak their gas to the exterior if they are connected to the surface (Figure 2). For simplicity, we call "continuous" and "dispersed" the gas phases from the former and latter types of bubbles, respectively, and evaluate their respective amounts of gas. The calculation is carried out at fragmentation and we discuss in Appendix A what happens to the "dispersed" gas phase later in the eruption sequence.

A simple argument illustrates the basic principle, and detailed calculations are deferred until Appendix B. Let us consider an initial volume of magma V_o which breaks up into N_f fragments of identical size r. We assume for simplicity that the fragments are spherical. By definition,

$$V_o = N_f \frac{4}{3}\pi r^3, \tag{1}$$

and the total volume of gas is

$$V_{\text{gas}} = \epsilon V_o, \tag{2}$$

where ϵ is the vesicularity of magma at fragmentation. We consider large fragments, which may be considered representative of the whole bubbly magma. The total volume of gas inside one such fragment is

$$V_{\text{in}} = \epsilon \frac{4}{3}\pi r^3. \tag{3}$$

If the mean bubble radius is b, bubbles located in a spherical shell of thickness $2b$ may be intersected by the fragmentation surface (Figure 3). This shell has volume

$$V_{\text{shell}} = 4\pi r^2 - 4\pi (r - 2b)^2 \approx 8\pi r^2 b. \tag{4}$$

One may consider that this shell has the same volume fraction of gas as the whole magmatic mixture. In the shell, some bubbles are not intersected by the fragmentation surface (Figure 3). Ignoring this for the moment, we obtain an upper bound on the amount of gas released at fragmentation:

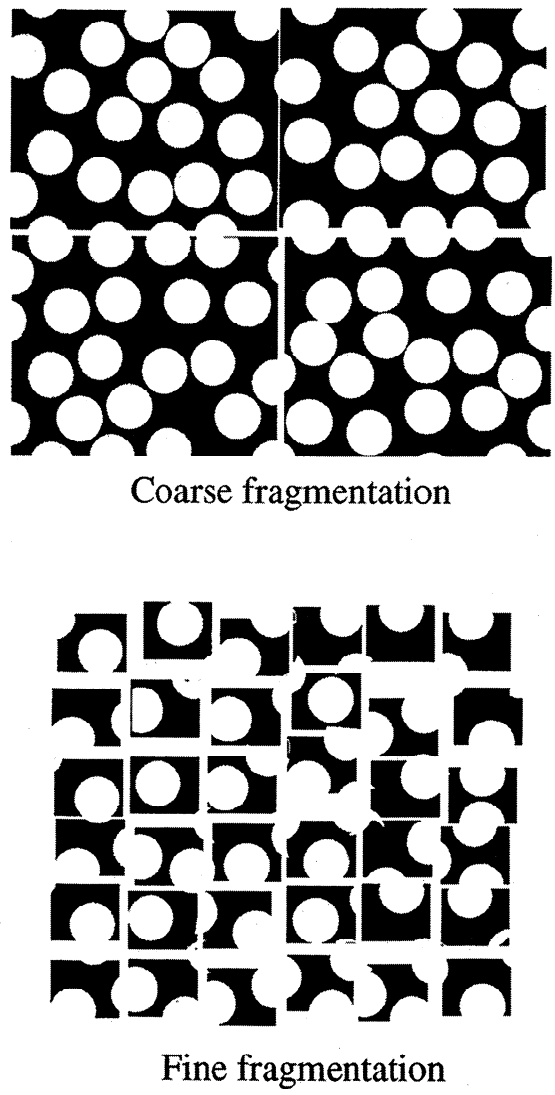

Figure 2. The size of fragments plays a critical role in determining the amount of gas released by fragmentation. Large fragments, which become pumices, preserve a large fraction of the exsolved gas. Small fragments, which become ash particles, do not retain any gas.

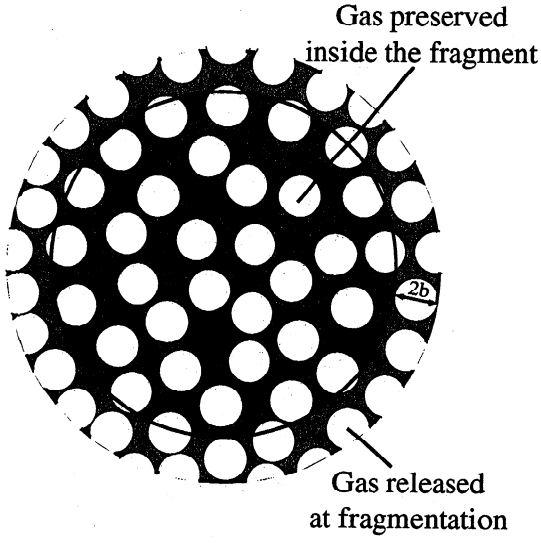

Figure 3. Sketch of a bubbly fragment at fragmentation. Gas bubbles may be split into two populations, depending on whether or not they are intersected by the fragmentation surface.

$$V_{\text{out}} \leq \epsilon\, V_{\text{shell}} = \epsilon\, 8\pi r^2 b, \tag{5}$$

which is rewritten as a fraction of the total amount of gas present:

$$\frac{V_{\text{out}}}{V_{\text{in}}} \leq \frac{6b}{r}. \tag{6}$$

Equation (6) shows how the fragment size comes into play: the larger the clast, the smaller the amount of gas released. In an explosive eruption, the sizes of magma fragments span a large range, and knowledge of the grain size distribution is needed for evaluating the mass of the continuous gas phase in the erupting mixture.

3. Fragment Populations in Pyroclastic Deposits

Pyroclastic deposits have been studied from different perspectives. Sedimentological techniques have been used to assess sorting processes as a function of wind velocity and mass discharge rate [e.g., *Fisher*, 1964]. *Walker* [1971] and *Pyle* [1989] have sought empirical ways to characterize deposits. *Wohletz* [1983] has attempted to link the size of pyroclasts to eruptive processes. Here, however, we are interested in the whole fragment population which is ejected from the eruptive vent, and in the mechanisms which are responsible for the size distribution of pyroclasts. We defer a discussion of fragmentation until the next section and summarize briefly a few important points.

Three size distribution functions, power law, lognormal, and exponential, are sufficient to account for almost all fragment populations generated in industrial and natural processes [e.g., *Redner*, 1990]. The lognormal distribution describes successfully droplets produced by the breakup of a liquid jet. Fragmenting a solid by an explosion or by hitting it with a hammer generates power law distributions. The exponential distribution, also called the Rosin-Hammer law, characterizes sequential processes such as grinding and milling. In a volcanological context, *Wohletz et al.* [1989] have used these distributions to study sorting and deposition in pyroclastic flows.

3.1. Method of Analysis

We have determined the size distribution of fragments from 25 pyroclastic fall deposits and 37 pyroclastic flow deposits using published data. Fragment sizes are usually determined by sieving and are given in ϕ units, such that

$$\phi = -\frac{\log d}{\log 2}, \tag{7}$$

where d is the maximum length of the fragment in millimeters. A few studies report data for the total clast population, which can be used directly. More frequently, this information is not available, and we have used the local grain size distribution and deposit thickness at different locations together with the isopach maps. We evaluate the total mass in sieve class ϕ, M_ϕ, by the volume integral

$$M_\phi = \int_0^L h(l)\, C_\phi(l)\, A(l) dl, \tag{8}$$

where $h(l)$ is the deposit thickness and $C_\phi(l)$ the concentration of class ϕ at distance l from the vent. ($A(l)\, dl$) is the area bounded by isopachs at distances l and $l+dl$, and L is the distance where h or C_ϕ drop to zero. We use linear interpolations for h and C_ϕ between localities.

We were able to find enough data for 25 fall deposits (Table 1). Two different data sets with slightly different size ranges are available for the Fogo A, Azores, deposit. The 1980 Mount St. Helens deposit is made of alternations of Plinian and coignimbrite ash layers. According to *Carey et al.* [1990], more than 77% of this deposit was erupted as pyroclastic flows and coignimbrite ash plumes and it was therefore classified as "coignimbrite." In several pyroclastic flow deposits, a global reconstruction of the fragment population is impossible because sieve data are reported for a small number of sites or because isopach maps are not given. For some of these, however, the grain size distribution appears to depend on distance only weakly, suggesting that deposition occurred en masse, that is, without significant sorting during lateral flow. In this case, we have averaged the grain size distributions reported, rejecting deposits where less than four different localities had been sampled. Results for 20 pyroclastic flow deposits are listed in Table 2. We have also used papers where the authors report data for a single "typical" sample assumed to be representative of the whole (Table 3). These data are clearly less reliable, but we found no systematic difference with the former category. They have been included for the sake

Table 1. Power Law Exponents for Pyroclastic Fall Deposits

Volcano Eruption	Deposit	Reference	D	$\Delta\phi$
Askja D, Iceland	Pl (G)	*Sparks et al.* [1981]	3.0***	[4;-9]
Chuseri, Japan	Pl (G)	*Hayakawa* [1985]	3.6***	[2;-5]
Hatepe, New Zealand	Pl (G)	*Walker* [1981a]	3.4***	[2;-4]
La Soufrière, French West Indies,	Subpl (G)	*Brazier et al.* [1982]	3.0**	[8;-2]
Nambu, Japan	Pl (G)	*Hayakawa* [1985]	3.7***	[0;-5]
Shikotsu, Japan	Pl (G)	*Katsui* [1959]	3.9**	[1;-5]
Tarumai, Japan	Pl (G)	*Suzuki et al.* [1973]	3.3***	[2;-5]
Taupo, New Zealand	Pl (G)	*Walker* [1980]	3.2***	[5;-3]
Waimihia, New Zealand	Pl (G)	*Walker* [1981a]	3.2***	[1;-4]
Fogo A, Azores	Pl(R)	*Walker and Croasdale* [1970]	3.1**	[3;-5]
Fogo A, Azores	Pl (R)	*Bursik et al.* [1992]	3.3***	[4;-5]
Fogo 1563, Azores	Pl (R)	*Walker and Croasdale* [1970]	3.2***	[1;-4]
Hudson, Chile	Pl (R)	*Scasso et al.* [1994]	3.3***	[10;-2]
Ksudach, Russia	Pl (R)	*Braitseva et al.* [1996]	3.4**	[5;-2]
Santa Maria , Guatemala	Pl (R)	*Williams and Self* [1983]	3.9**	[5;-5]
Toluca, Mexico	Pl (R)	*Bloomfield et al.* [1977]	3.4**	[4;-5]
	Pl (R)	*Bloomfield et al.* [1977]	3.5**	[4;-5]
Mount St. Helens, United States	Coig (G)	*Carey and Sigurdsson* [1982]	3.7***	[9;-4]
Askja C, Iceland	PhPl (G)	*Sparks et al.* [1981]	3.5***	[5;-7]
Hachinohe, unit 1, Japan	PhPl (G)	*Hayakawa* [1985]	3.5***	[9;-2]
Hachinohe, unit 2	PhPl (G)	*Hayakawa* [1985]	3.5***	[9;-3]
Hachinohe, unit 3	PhPl (G)	*Hayakawa* [1985]	3.5***	[9;-3]
Hatepe ash, New Zealand	PhPl (G)	*Walker* [1980]	3.2**	[9;-3]
	PhPl (G)	*Walker* [1981b]	3.1**	[9;-3]
Rotongaio, New Zealand	PhPl (G)	*Walker* [1980]	3.5**	[9;-3]
Wairakei, New Zealand	PhPl (G)	*Self* [1983]	3.3**	[8;-1]

Abbreviations are G, total population given by the author; R, population reconstructed using isopachs and local distributions at various sites; Pl, Plinian deposit; SubPl, SubPlinian deposit; PhPl, phreato-Plinian deposit; Coig, coignimbrite ash.
$\Delta\phi$, range of sieve units for the data.
* Indicates reasonable agreement with a power law.
** Excellent agreement with a power law in the intermediate size range, and small deviations at small and large sizes.
*** Excellent agreement with a power law distribution over the whole size range.

of completeness. The total number of pyroclastic flow deposits available for study is 37.

In order to calculate the number of fragments, we divide the total mass in each sieve class by the average fragment mass. This requires knowledge of the fragment density ρ^*, which may not be the same for all sieve classes. As the sieve aperture diminishes, the fragment density tends to increase [*Walker*, 1980]. This reflects the fact that a small fragment does not contain a large number of bubbles and hence is not representative of the whole magma/bubble mixture. We know that fragments with radii smaller than the bubble radius b cannot contain any gas. Large fragments sample the average mixture, and their densities are expected to be independent of size. This has indeed been verified for fragments larger than about 1 cm [*Houghton and Wilson*, 1989; *Gardner et al.*, 1996]. For fragments smaller than this, we assume that the fragment vesicularity ϵ^* depends on fragment radius r as follows:

$$\epsilon^* = \epsilon\,(1 - r_c/r)\,, \quad r \geq r_c\,, \tag{9}$$

$$\epsilon^* = 0, \quad r \leq r_c\,, \tag{10}$$

where r is the fragment radius and ϵ is the average vesicularity of the mixture. Limit radius r_c is related to the average bubble size. Fragments much larger than r_c are representative of the whole mixture, and fragments smaller than r_c are devoid of vesicles. Using (9), the density of a fragment ρ^* is given by

$$\rho^* = \rho_l\,(1 - \epsilon^*) + \rho_g \epsilon^* \approx \rho_l\,(1 - \epsilon^*)\,, \tag{11}$$

where ρ_l is the magma density and ρ_g is the gas density. Throughout the following we have taken $r_c = 10^{-4}$ m and $\epsilon = 75\%$. We calculate the total number of fragments in the sampled population and deduce the fraction represented by each sieve class. This normalization procedure ensures that the results are independent of the specific value taken for magma density. The results are weakly sensitive to the other two parameters, r_c and ϵ, provided that their values are chosen within realistic ranges. As we shall see, the size distributions can be characterized accurately using data at intermediate grain sizes, for which no correction is required.

3.2. Power Law Distributions

Grain size distributions for the Plinian populations at Askja, Iceland [*Sparks et al.*, 1981], and Hachinohe, Japan [*Hayakawa*, 1985], are shown in Figure 4. Data from the Taupo ignimbrite, New Zealand [*Walker and*

Table 2. Power Law Exponents for Pyroclastic Flow Deposits: Whole Deposits

Volcano Eruption	Deposit	Reference	D	$\Delta\phi$
Merapi, Indonesia	Ig (G)	*Boudon et al.* [1993]	2.9**	[6;-6]
Taupo, New Zealand	Ig (G)	*Walker and Wilson* [1983]	3.3***	[5;-6]
Acatlan, Mexico	Ig (R)	*Wright and Walker* [1981]	2.9**	[5;-5]
Aira, Japan	Ig (A-13)	*Murai* [1961]	3.2*	[9;-8]
Akan, Japan	Ig (A-4)	*Murai* [1961]	2.9**	[9;-7]
Asamayama, Japan	Ig (A-38)	*Murai* [1961]	3.1*	[9;-9]
Hakone, Japan	Ig (A-13)	*Murai* [1961]	3.0**	[9;-9]
Harunasan, Japan	Ig (A-4)	*Murai* [1961]	3.1*	[9;-7]
Ko-Fuji, Japan	Ig (A-10)	*Murai* [1961]	3.0*	[9;-9]
Komagatake, Japan	Ig (A-10)	*Murai* [1961]	3.0**	[9;-8]
Kusatsu-Shiranesan, Japan	Ig (A-4)	*Murai* [1961]	3.0**	[9;-7]
Kutcharo, Japan	Ig (A-10)	*Murai* [1961]	3.1**	[9;-6]
Monte Pilato, Lipari, Italy	Ig (A-21)	*Dellino and La Volpe* [1995]	3.1***	[6;-6]
	S (A-13)	*Dellino and La Volpe* [1995]	3.2**	[6;-6]
Nantaisan, Japan	Ig (A-6)	*Murai* [1961]	2.9**	[9;-7]
Rabaul, Papua New Guinea	Ig (A-27)	*Walker* [1981b]	3.2**	[9;-6]
	Ig (A-10)	*Walker* [1981b]	3.2**	[9;-6]
Shikotsu, Japan	Ig (A-11)	*Murai* [1961]	3.1*	[9;-6]
Tokachidake, Japan	Ig (A-8)	*Murai* [1961]	3.0**	[9;-9]
Toya, Japan	Ig (A-10)	*Murai* [1961]	3.2**	[9;-6]
Towada, Japan	Ig (A-22)	*Murai* [1961]	3.2**	[9;-8]

Abbrevations are G, total population given by the author; R, population reconstructed using isopachs and local distributions at various sites; A-n, average of n local populations; Ig, ignimbrite; S, surge deposit.
$\Delta\phi$, range of sieve units for the data.
* Indicates reasonable agreement with a power law.
** Excellent agreement with a power law in the intermediate size range, and small deviations at small and large sizes.
*** Excellent agreement with a power law distribution over the whole size range.

Wilson, 1983], are represented in Figure 5. For all the deposits studied, save for the single exception of the 79 A.D. Vesuvius, Italy, Plinian deposit, we find that the number of fragments in each sieve class ϕ, $\Delta(\phi)$, follows closely the following equation:

$$\ln_2[\Delta(\phi)] = \ln_2[N_o] - D\phi, \quad (12)$$

where N_o is a normalization constant. This equation reflects a power law size distribution [*Hartmann*, 1969]:

$$N(R \geq r) = \lambda r^{-D}, \quad (13)$$

where $N(R \geq r)$ is the number of fragments greater than r, and λ is a normalization constant.

In the 62 deposits used for this paper, the available size range extends over at least six ϕ units, typically from 0.12 to 8 mm ($3 \geq \phi \geq -3$), which is sufficient for a reliable analysis. The exponent of the power law distribution was obtained using a least squares fit to the data. We estimate that the error does not exceed ± 0.1 using departures from the best fit power law and by repeating the analysis for various subsets of the data. Using either the coarse fraction (larger than 1 mm), or the fine fraction (less than 1 mm), led to the same power law exponent. We evaluate the consequences of errors in the data by calculating the total mass of the deposit

$$M_{\text{tot}} = \int_{r_{\min}}^{r_{\max}} \frac{4}{3}\pi\rho r^3 dN(r) = \int_{r_{\min}}^{r_{\max}} \frac{4}{3}\pi\rho r^3 \lambda(-D) r^{-D-1} dr, \quad (14)$$

where $r_{\min}$ and $r_{\max}$ are the lowest and largest size of the distribution. For $D \neq 3$,

$$M_{\text{tot}} = -\lambda \frac{4}{3}\pi\rho \frac{D}{D-3}\left[r_{\max}^{3-D} - r_{\min}^{3-D}\right]. \quad (15)$$

We split this mass into two contributions from fragments larger and smaller than the middle size $(r_{\min} + r_{\max})/2$, and calculate their ratio. For pyroclast populations, values of D are close to 3, and adding or subtracting 0.1 to the best fit D value acts to change the mass ratio by a factor of about 2. This shows that it takes gross changes in the sieve data to affect the exponent value.

In the tables we have rated how well the size data fit a power law. Pyroclastic fall deposits are generally excellent. Pyroclastic flow deposits tend to be less satisfactory, which may be attributed to imperfect data coverage. For those few flow deposits where enough data are available to reconstruct the whole fragment population, the agreement with a power law size distribution is excellent. The nature of the data available raises two different issues. One issue is whether pyro-

Table 3. Power Law Exponents for Pyroclastic Flow Deposits: Single Samples

Volcano Eruption	Deposit	Reference	D	$\Delta\phi$
Altavilla, Italy	Ig	*Walker* [1971]	3.4**	[5;-5]
Angra, Azores	Ig	*Walker* [1971]	3.1**	[5;-5]
Atitlan, Guatemala	Ig	*Walker* [1971]	3.2**	[5;-5]
Granadilla, Canary Islands	Ig	*Booth* [1973]	3.3***	[5;-5]
Hakkadasan, Japan	Ig	*Murai* [1961]	3.2**	[9;-8]
Herculaneum, Italy	Ig	*Walker* [1971]	3.1**	[5;-4]
Krakatau, Indonesia	Ig	*Carey et al.* [1996]	3.3**	[10;-5]
	Ig	*Carey et al.* [1996]	3.2***	[10;-5]
Ngauruhoe, New Zealand	Ig	*Nairn and Self* [1978]	3.0**	[4;-6]
	Ig	*Nairn and Self* [1978]	2.9**	[4;-6]
Numajiri, Japan	Ig	*Murai* [1961]	3.0**	[9;-9]
Osoreyama, Japan	Ig	*Murai* [1961]	3.0**	[9;-5]
Povoacão, Azores	Ig	*Walker* [1971]	2.9**	[5;-5]
San Mateus, Azores	Ig	*Walker* [1971]	3.1**	[5;-5]
Takaharayama, Japan	Ig	*Murai* [1961]	3.2**	[9;-6]
Tazawa, Japan	Ig	*Murai* [1961]	3.1**	[9;-6]
Tokachi, Japan	Ig	*Murai* [1961]	3.0**	[9;-9]

Data for a single representative sample in a deposit.
Ig, ignimbrite.
$\Delta\phi$, range of sieve units for the data.
** Excellent agreement with a power law in the intermediate size range, and small deviations at small and large sizes.
*** Excellent agreement with a power law distribution.

clastic populations can be characterized by a power law over the whole size range. The other issue is that we are interested in clast sizes in the volcanic conduit, but only sample fragments which have accumulated in a deposit. Thus we must assess whether the fragment population gets modified once it has left the eruptive vent.

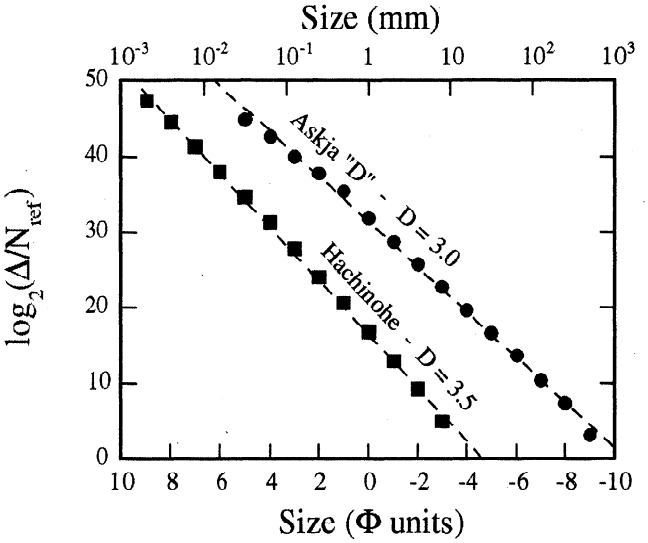

Figure 4. Grain size distribution for the Hachinohe, Japan, and Askja, Iceland, Plinian deposits (data from *Sparks et al.* [1981] and *Hayakawa* [1985]). Data are shown as the number of fragments in each sieve class $\Delta(\phi)$ normalized by an arbitrary constant N_{ref}, as a function of size. Sieve unit ϕ is such that the particle diameter is $2^{-\phi}$ mm. The slope of $\ln_2[\Delta(\phi)]$ versus ϕ is the power law exponent D.

3.3. Bias in the Data

In some cases (identified in the tables), we found small deviations from the best fit power law for small and large sizes. One example from the Rotongaio fall deposit, New Zealand [*Walker*, 1981b], is illustrated in Figure 6. Such anomalies appear as deficits and may be attributed to various causes. A sampling problem is encountered for large fragments, with radii larger than a few tens of centimeters ($\phi \leq -6$). Such fragments represent a very small fraction of the total deposit, and hence a representative sample would require sieving enormous volumes in the field. The main problem, however, is for fine particles.

The finest fraction of an ash and pumice population is often lost to the atmosphere, [e.g., *Wiesner et al.*, 1995]. Furthermore, as noted by *Sparks et al.* [1981], distal ash deposits may be eradicated soon after deposition, by rain, for example. In fact, the data for very small sieve classes are seldom measured in the field, and are frequently obtained by extrapolation. For example, *Walker* [1981b] determined isopachs for a number of sieve classes and used an extrapolation technique to infer the positions of isopachs for smaller fragments. On the one hand, this may be considered problematic because the amount of fines is not measured directly. On the other hand, the fines are usually missing from the deposit and this procedure allows a reconstruction. Nevertheless, it is clear that deviations from the power law may be due to uncertainties in the extrapolation technique.

Where it has been demonstrated, the loss of fragments is significant only for sizes smaller than 0.5 mm

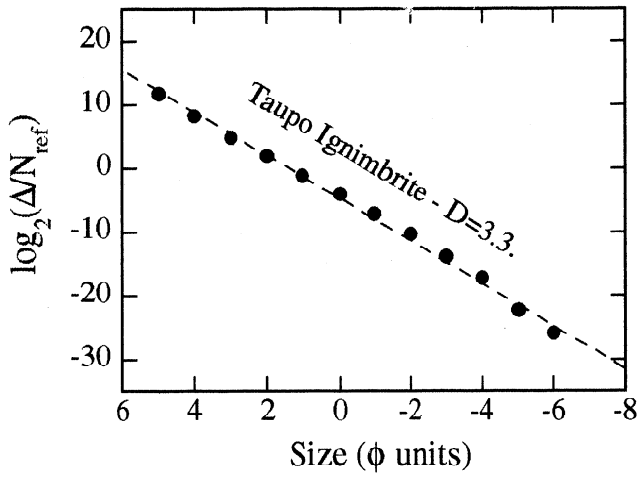

Figure 5. Grain size distribution for the Taupo ignimbrite, New Zealand (data from *Walker and Wilson* [1983]). Data are shown as the number of fragments in each sieve class $\Delta(\phi)$ normalized by an arbitrary constant N_{ref}. Sieve unit ϕ is such that the particle diameter is $2^{-\phi}$ mm. A power law distribution allows an excellent fit to the data.

($\phi \geq 1$) [e.g., *Wright and Walker*, 1981]. Some deposits with very large proportions of fines, that is, with large D values, are available. For some of those, the data available span an extremely large size range (from 9 to -3 ϕ units at Hachinohe, and from 9 to -4 at Mount St. Helens, Table 1), and there is no detectable change of power law exponent at some intermediate size. This shows that both the coarse and fine fractions are characterized by the same size distribution, and hence that the coarse fraction ($\phi \leq 1$, i.e. $d \geq 0.5$ mm) is sufficient to characterize the whole population. We have emphasized above that it takes large errors in the sieve data to affect the exponent value. For the power law exponents found here, the missing fine fraction must represent more than 50% of the total deposit mass to affect the results significantly.

The problem of missing fines is difficult to solve, and one must ask what is the best method to reconstruct the fine fraction. This fraction cannot be recovered, and the various assumptions which have been made are impossible to test. One procedure is to extrapolate isopach maps [e.g., *Walker*, 1981b], which implies an hypothesis on settling conditions. Other procedures based on the systematics of field data have been adopted, as discussed below. In other scientific fields, a common method has been to use the size distribution itself, and, more specifically, power law distributions [*Cargill et al.*, 1981; *Turcotte*, 1992, pp. 58-63]. The missing fractions are estimated by extrapolating the best fit distribution established over an intermediate size range. We note that deviations from a power law distribution tend to decrease when the sampling is more extensive, and that power law distributions have been found for many other fragment populations which could be comprehensively sampled [*Redner*, 1990]. In fact, pyroclast populations tend to be closer to power law size distributions than many of these other populations [e.g., *Ranz*, 1959; *Hartmann*, 1969]. We shall show later in this paper that the fragmentation of bubbly magma does generate power law size distributions.

3.4. Coignimbrite Ash Layers

Pyroclastic flows often generate secondary ash plumes which generate coignimbrite ash layers scattered over a wide area. Such layers may be easily remobilized and eradicated, implying that, in some cases, a flow deposit may only account for part of the total fragment population ejected from the vent. Two methods have been used to correct for this. Stratigraphic studies of a deposit may reveal changes of size distribution as a function of height. Typically, one may observe that upper units are depleted in fines with respect to the base. Such size grading affects mostly fragments smaller than 0.5 mm ($\phi \geq 1$) [*Wright and Walker*, 1981]. Using a reference unit unaffected by sorting and loss of fines, the other units can be reconstructed empirically. An alternative method is to use the initial crystal content of the magma determined from the coarsest pumices. Fragmentation effectively separates small magma fragments and crystals, and subsequent ash loss leads to layers which are anomalously crystal rich [*Sparks and Walker*, 1977]. One may reconstruct each sieve class by bringing the crystal content back to its original magmatic

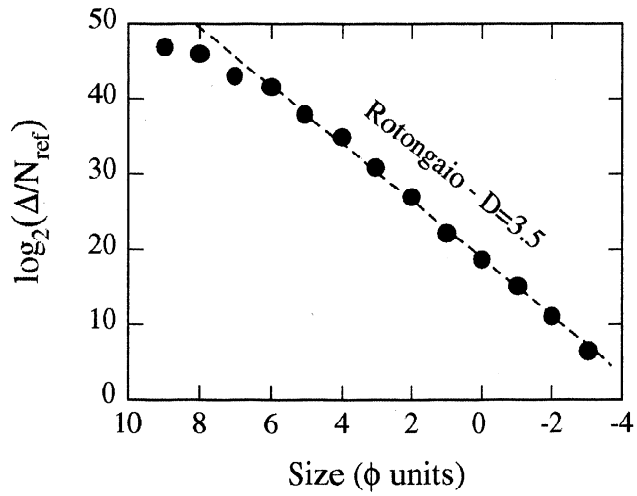

Figure 6. Grain size distribution for the Rotongaio ash deposit, New Zealand (data from *Walker* [1981b]). Data are shown as the number of fragments in each sieve class $\Delta(\phi)$ normalized by an arbitrary constant N_{ref}. Sieve unit ϕ is such that the particle diameter is $2^{-\phi}$ mm. In an intermediate size range spanning 3 orders of magnitude, the data are consistent with a power law with exponent D=3.5. The data for the smallest sizes deviate from this power law. These data have been estimated by extrapolating the positions of isopachs for large grain sizes.

value. Such a correction has been applied to the Taupo ignimbrite [*Walker and Wilson*, 1983], where it is estimated that about 45 % of the total erupted material has been lost. The significance of this estimate may be assessed using the error analysis given above, where we showed that changing the D value by 0.1 requires changing the proportions of the coarse and fine fractions by a factor of about 2. The uncorrected Taupo ignimbrite data lead to $D = 3.2$, whilst the corrected data lead to $D = 3.3$. The corrected data are in remarkable agreement with a power law distribution throughout the size range available (Figure 5).

3.5. Changes of Size Distribution During Deposition

Pumices may break up when hitting the ground or as they get buried in a thick deposit. If late breakage is predominant, the local grain size distribution in a deposit should not depend on distance. In near-source Plinian deposits, the majority of coarse clasts are broken by impact [*Sparks et al.*, 1981]. The influence of impact decreases away from source and impact breakage is unimportant for clasts less than a few centimeters in diameter ($\phi \geq$ -5). The very coarse fraction ($\phi \leq$ -5) is seldom used (Tables 1-3). Away from source, the local grain size distribution of a Plinian deposit varies systematically as a function of distance, as predicted by quantitative models of settling from an umbrella cloud [*Bursik et al.*, 1992; *Koyaguchi*, 1994]. The agreement between theory and observation indicates that deposition does not affect significantly the global Plinian grain size distribution.

In a pyroclastic flow, fragments are susceptible to abrasion and refragmentation over the whole length of the deposit [*Wohletz et al.*, 1989]. It is difficult to evaluate the importance of these effects with an a priori physical model and the best method would be to compare deposits with different emplacement characteristics. This is not feasible with the present data set for lack of information, but we note that a surge deposit from Monte Pilato, Italy [*Dellino and La Volpe*, 1995] has almost the same power law exponent as the associated flow deposit (Table 2). Furthermore, we will show that if late refragmentation is indeed significant during lateral transport at the surface, the result should be an increase of the D value. Thus the values of D from the deposits provide upper bounds for the values of D at the vent. This point must be born in mind for later discussions.

3.6. D Values of Pyroclastic Deposits

Values of exponent D for the different fall deposits studied are between 3.0 and 3.9 (Table 1), that is, are always greater than 3. Figure 7 indicates that the pyroclastic flow exponents are systematically smaller than the fall exponents. As will be discussed later, this finding is important and it would be desirable to base it on firmer ground with more detailed and comprehensive studies of flow deposits. Nevertheless, it is significant that, in all the papers we have consulted, we were not able to find a single flow sample with $D > 3.4$ (Tables 2 and 3) and that the D values for flow deposits are clustered around 3.1. At Taupo, even after correction for the loss of fines, the ignimbrite is clearly coarser than the Plinian deposit from the same eruption [*Walker and Wilson*, 1983]. Another observation is that there are no populations with exponents smaller than 2.9, which is also significant, as discussed below. A final remark is that the exponents span a rather large range. The different D values are not due to poor resolution or to errors in the best fit procedure, as emphasized by Figure 4, which shows that the two best Plinian data sets lead to D values of 3.0 and 3.5.

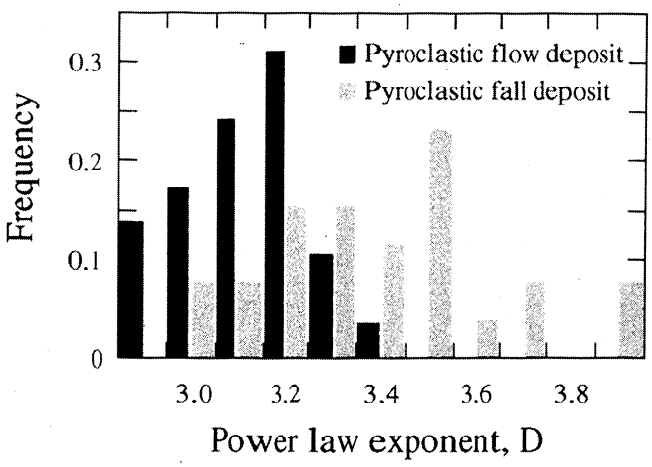

Figure 7. Histograms of the power law exponents for the deposits listed in Tables 1, 2, and 3.

The exponent of the power law distribution provides a convenient and precise way to characterize pyroclastic populations, which can be compared to bulk eruption characteristics. For example, we have found that, in Plinian eruptions, the D value is not correlated to the mass discharge rate.

4. Physical Processes of Fragmentation

4.1. Previous Studies

There are a large variety of and a vast literature on fragmentation processes [see *Redner*, 1990], and it is impossible to do justice to this topic here. It is important to distinguish between "primary" breakup, such that the starting material is split into individual fragments, and "secondary" breakup, such that the primary fragments get refragmented. "Primary" size distributions have been determined empirically and have been justified from the physics of the breakup process in a few cases only. Theoretical efforts have been focused on continuous fragmentation, where the size distribution evolves due to repeated "secondary" breakup. Most

studies have dealt with the fragmentation of dense material, either solid [*Turcotte*, 1986] or liquid [*Ranz*, 1959], and pyroclasts offer the different case of fragments derived from highly vesicular liquid with void fractions in excess of 60% [*Gardner et al.*, 1996].

Any analysis must start with the "primary" breakup process and its associated size distribution. Key variables are the material properties, sample geometry, and the energy input. The latter has the most important effect. At small energy input, only small pieces can be broken at the surface of the sample. At medium energy input, a small number of fragments are generated, whose sizes remain close to those of the initial sample. At large energy input, all flaws and heterogeneities in the sample may be "activated" and a wide range of fragment sizes may be generated. The data available indicates that, for a wide variety of materials and breakup processes, fragment sizes follow power law distributions with a very narrow range of exponents [*Redner*, 1990]. The largest size is a function of the initial sample dimensions and the smallest size is controlled by the scale of flaws and heterogeneities in the sample. In the case of vesicular magma fragments, flaws are easily identified: they are the bubbles themselves. Indeed, the smallest ash particles are remnants of vesicle walls [*Fisher and Schmincke*, 1984].

Hartmann [1969] and *Turcotte* [1986] have shown that any "primary" breakup process which is scale invariant generates power law exponents between 2 and 3. The macroscopic self-similar power law distribution may be derived for specific failure models, such as the generation of weak planes, for example [*Allègre et al.*, 1982; *Turcotte*, 1986]. For each type of failure, there exists a critical concentration of defects for which catastrophic fragmentation occurs. This critical probability is macroscopically related to the power law exponent of the fragment population [*Turcotte*, 1986]

$$p_c = 2^D/8. \tag{16}$$

This probability cannot be larger than 1, which implies that the power law exponent must be smaller than 3. In this theory, the breakup of a fragment of size r generates 2^D fragments of size $r/2$ [*Turcotte*, 1986]. Mass conservation requires that a fragment of size r cannot generate more than eight fragments of size $r/2$ and hence that the maximum D value is 3.

A key property of pyroclast populations is their large size range, spanning 6 orders of magnitude from micron-sized ash particles to meter-sized pumice blocks. *Gardner et al.* [1996] have shown that, for pyroclasts larger than 1 cm, vesicularity values and fragment shapes are scale invariant. It would be natural to expect that the volcanic fragmentation process is also scale invariant. Pyroclastic populations are indeed characterized by power law size distributions, but their exponents are generally larger than 3.0 (Table 1). Another peculiarity of pyroclastic populations is the large spread of D values. One would expect a single value of the exponent corresponding to the specific breakup process at work. We have made an extensive literature search and have found no "primary" fragmentation event capable of generating such peculiar features. One may propose two explanations. One is that the pyroclastic size distribution is related to the bubble size distribution, which may vary between different magmas and different eruptions. Another explanation is that it is due to secondary fragmentation. In order to evaluate these, we have carried out a series of fragmentation experiments in the laboratory on volcanic materials. The experiments are not meant to reproduce the true mechanism of fragmentation at work in a volcanic eruption, but to illustrate the basic mechanisms involved.

4.2. Laboratory Experiments: Primary Fragmentation

We have used rhyolitic pumices from the Minoan Plinian deposit in Santorini, which have a range of vesicularities [*Gardner et al.*, 1996]. A piston was dropped once onto a large Minoan sample and induced fragmentation. The size distribution, determined by sieving, fits a power law with an exponent of about 2.7 (Figure 8). This value is close to those found for a variety of explosion or shattering phenomena [*Turcotte*, 1986]. In the piston experiments, the energy supply is large, implying no limitation on the size and type of defects which may get activated within the material. A different fragmentation mechanism is bubble expansion and coalescence due to decompression. In this case, energy originates

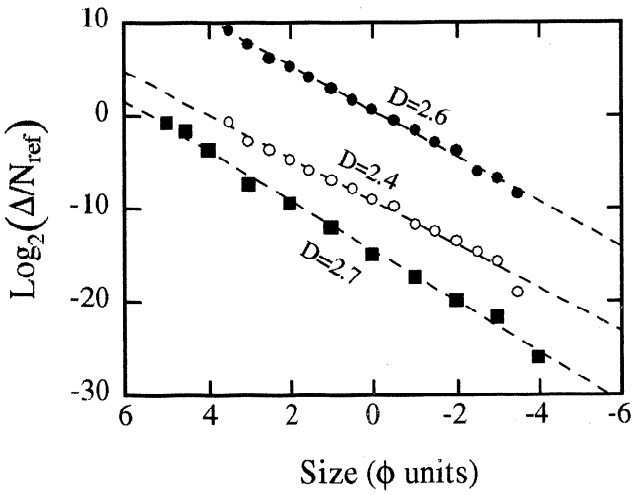

Figure 8. Grain size distribution due to primary fragmentation events. Data are shown as the number of fragments in each sieve class $\Delta(\phi)$ normalized to an arbitrary constant N_{ref}. Sieve unit ϕ is such that the particle diameter is $2^{-\phi}$ mm. Circles correspond to rapid decompression experiments on viscous magmas [*Alibidirov and Dingwell*, 1996]. Plain squares correspond to the breakup of a Minoan pumice hit once by a piston.

from within the starting material and its amount depends on the magnitude of the pressure drop.

We have made foaming experiments using an analog material, a solution of acetone and Gum-Rosin [*Phillips et al.*, 1995]. This material shares many properties with volatile-rich silicate melts, and in particular large increases of melt viscosity as degassing proceeds. We placed a sample of acetone-rich Gum-Rosin sample in a vacuum chamber capped by a spherical glass cap and decreased pressure. The liquid foamed and fragmented, sending out small liquid droplets which were collected on the glass cap. We measured their sizes and found a lognormal distribution, which is typical of pure liquid fragmentation [*Ranz*, 1959].

Alibidirov and Dingwell [1996] carried out sudden decompression experiments on natural rhyolitic melts at high temperature. Fragmentation was induced by a shock wave propagating through the highly viscous samples. In these experiments, the pressure drop and the decompression rate were much larger than in the foaming experiments just described. Using data from two independent experiments, we have found power law size distributions with values of 2.4 and 2.6 for the exponent (Figure 8). The number of fragments generated in these experiments is rather small and these two values cannot be considered significantly different from one another, and different from the 2.7 value obtained in the piston experiment. These results suggest that the fragment size distribution depends neither on the fragmentation mechanism nor on bubble size. These different fragmentation experiments generate power law size distributions with exponents smaller than 3, confirming the existing body of experimental data on all kinds of "primary" breakup mechanisms. To account for the characteristics of pyroclastic deposits, we therefore look for "secondary" fragmentation processes.

4.3. Laboratory Experiments: Secondary Fragmentation

"Secondary" fragmentation occurs, for example, during milling and in gaseous atomizers. The gaseous atomizer is of particular interest because it shares many characteristics with an explosive volcanic eruption. In this device, liquid droplets are injected into a turbulent gas flow and are broken up by turbulence, leading to a power law size distribution with an exponent larger than 3 [*Ranz*, 1959]. This result has been explained by selective refragmentation [*Dombrowski and Johns*, 1963; *Hinze*, 1955; *Reitz and Bracco*, 1982; *Silverman and Sirignano*, 1994]. Large droplets deform more easily than small ones, and hence refragment preferentially, which acts to increase the proportion of fines in the population.

We have induced selective refragmentation in Minoan pumice in the following manner. A large sample was fragmented with a piston, as above. The resulting fragment population had a power law exponent of 2.7 and was separated in three groups. The first group was refragmented several times with the same piston. The size distribution of the fragment population was evaluated after each strike (Figure 9a). We found that, in this case, the population always keeps the same power law exponent of 2.6 ± 0.1, which is equal to the initial value. The reason for this is that, at each strike, each fragment breaks up because of the large energy imparted by the piston, implying that there is no preferential refragmentation. The second group of pumice fragments was placed in a grinder (a rapidly rotating chamber) from which steel balls had been removed. The experiment was stopped at successive times and the size distribu-

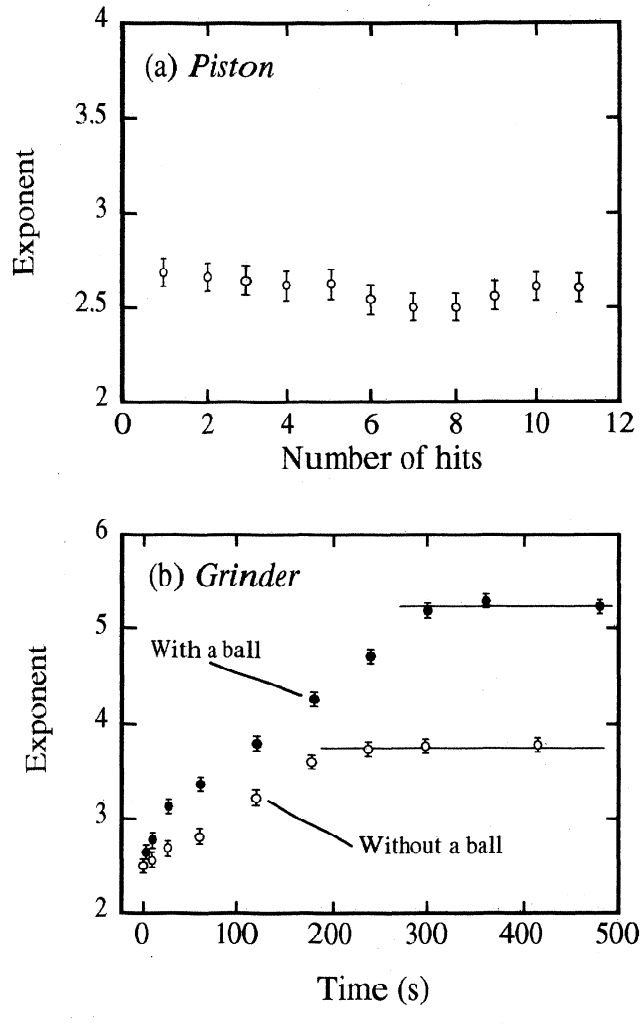

Figure 9. (a) The power law exponent of fragments produced by repeatedly dropping a piston onto the same Minoan pumice. Data are shown as a function of the number consecutive "hits" by the piston. There is no change because each hit breaks up all the fragments present. (b) The power law exponent of Minoan pumice fragments produced in a grinder (a rapidly rotating chamber) as a function of time. In one experiment, fragmentation is induced by collisions between fragments as well as against the grinder walls. In the other experiment, a steel ball is added to the charge, adding a third fragmentation agent.

tion was determined as a function of time. The power law exponent increased with time until it seemed to reach a steady state value of about 4.2 (Figure 9b). In a third and final experiment, we placed a small steel ball in the grinder. We found the same trend of increasing power law exponents, but the values were larger than in the experiment without a steel ball. The time to reach steady state was larger and the final exponent was also larger (5.4 instead of 4.2). "Secondary" fragmentation was therefore more efficient in this case, which suggests that the power law exponent is sensitive to the energy available in collision events.

The experiments demonstrate that it is indeed possible to change a power law exponent from an initial value smaller than 3 to a value larger than 3. Such "secondary" fragmentation mechanisms may be called "kinetic" because they involve the timescale of fragment collisions. We now develop a simple analytical model to illustrate how selective refragmentation can change the value of a power law exponent.

4.4. Model of Selective Kinetic Refragmentation

We first consider a "primary" fragment population, described by a power law distribution. If a block of size r' is fragmented, the resulting population is described by

$$N(R > r) = g(r, r') = f(r')\, r^{-D_i}, \tag{17}$$

where $f(r')$ is some function of the initial sample size r', and D_i is the "primary" power law exponent. Function $f(r')$ is calculated using mass conservation:

$$r'^3 = f(r') \int_0^{r'} (-D_i) r^{-D_i - 1} r^3 dr, \tag{18}$$

This integral diverges if D_i is larger than 3.0 or must be calculated over a finite range. Substituting for $f(r')$, we obtain

$$N(R > r) = g(r, r') = \frac{D_i - 3}{D_i} \left(\frac{r}{r'}\right)^{-D_i}. \tag{19}$$

Here the size distribution of fragments depends explicitly on the initial sample size r'.

For refragmentation, the number of fragments of a given size depends on the size distribution of "primary" fragments as well as on the probability of refragmentation. The critical ingredient is that this probability depends on fragment size. The number of fragments of size r at time t, $dN(r,t)$, is the solution of [*Cheng and Redner*, 1990]

$$\frac{\partial dN(r,t)}{\partial t} = -a(r,t)\, dN(r,t) + \int_r^\infty a(r',t)\, dN(r',t)\, g(r,r'), \tag{20}$$

where $a(r,t)$ is the probability of refragmenting clasts with size r at time t.

We look for a self similar solution such that the power law exponent does not depend on time, which corresponds to the steady state regime of the grinder experiments

$$dN = \lambda(-D_f)\, r^{-D_f - 1} dr, \tag{21}$$

where D_f is the final steady state exponent. For the probability of refragmentation, we look for functions of the following form:

$$a(r) = r^C, \tag{22}$$

where C is an a priori unknown positive parameter. Substituting for (19) and (21) in (20) at steady state, we obtain

$$r^{C+1+D_i-D_f-1} = (D_i - 3) \int_r^\infty r'^{C+D_i-D_f-1} dr'. \tag{23}$$

This integral converges if $D_f \geq C + D_i$. If this condition is met, we obtain

$$r^{C-D_f+D_i} = r^{C-D_f+D_i} \frac{D_i - 3}{D_i - D_f + C}, \tag{24}$$

which implies that

$$D_f = 3 + C. \tag{25}$$

This solution requires that $D_f \geq C + D_i$, implying that $D_i < 3$, which was our initial assumption. This simple argument demonstrates that the final exponent can indeed be greater than 3, independently of the initial exponent.

Solving for the refragmentation probability requires a sophisticated model of fragment interactions and collisions, which would be outside the scope of the present work. The simplest hypothesis is that this probability is related to the fragment cross section, that is, that

$$a(r) \propto r^2. \tag{26}$$

This corresponds to C=2 and to a final exponent of 5, which is comparable to the steady state values of the grinder experiments. The value of C also depends on the efficiency of collisions, which probably increases with the size of impacting fragments. A final effect is that, as their size goes down, particles are probably less and less susceptible to breakage because they contain fewer and fewer defects [*Redner*, 1990]. This may be included in the probability function $a(r)$. With highly porous material such as pumices, additional factors come into play. With increasing D value, the amount of continuous gas increases, as emphasized above. Fragment collisions become less frequent, and the size distribution may evolve increasingly slowly towards the asymptotic D value.

5. Volcanic Fragmentation

We now piece together the constraints obtained on the size distribution of pyroclastic populations and on the nature of fragmentation processes and discuss implications for volcanic flows.

5.1. Amount of Continuous Gas in the Volcanic Mixture

To calculate the amount of gas released for the true fragment populations determined above, the extreme fragment sizes are chosen to be 1 m (a fragment size which has been found close to vent on several occasions) and 1.5 μm. The latter value is compatible with the 1 μm value commonly used for reconstructing deposits [*Walker*, 1973, 1981b], and the 1.42 μm value proposed by *Pyle* [1989] from several independent observations. It is sufficient to consider a single bubble size b. It is shown in Appendix B that results are not changed appreciably by more complex bubble size distributions and are weakly sensitive to the mean bubble size, provided it is chosen within a realistic range.

The total mass of a deposit is given by (15). The sizes of the smallest and largest fragments, $r_{\min}$ and $r_{\max}$, differ by as much as 6 orders of magnitude, and hence only one term on the right-hand side of this equation dominates, depending on the sign of $(3 - D)$. If D is greater than 3,

$$M_{\text{tot}} \propto r_{\min}^{3-D}. \tag{27}$$

In this case, the population is controlled by the fine fraction, implying that most of the gas gets released at fragmentation. On the other hand, if D is less than 3, the total mass is

$$M_{\text{tot}} \propto r_{\max}^{3-D}. \tag{28}$$

In this case, most of the deposit is made of coarse fragments, implying that a small amount of gas is released at fragmentation.

The fraction of gas released at fragmentation is given in Figure 10 as a function of D for $b = 10^{-4}$ m. For $D > 3.5$, almost all the gas is released at fragmentation. For $D < 2.8$, a negligible amount of gas is released. In this latter case, the mixture of gas and vesicular fragments is best described as a dense granular mixture. Around the critical value of 3, small changes of the exponent induce extremely large variations of the amount of gas released. Increasing the exponent from 3.0 to 3.5 acts to increase this amount from about 40% to 90% of the available gas. "Complete atomization" is therefore a reasonable approximation only for exponents larger than 3.5, which is a relatively rare occurrence observed only in fall deposits. As indicated by the laboratory experiments, such large values of the power law exponent are not achieved at fragmentation.

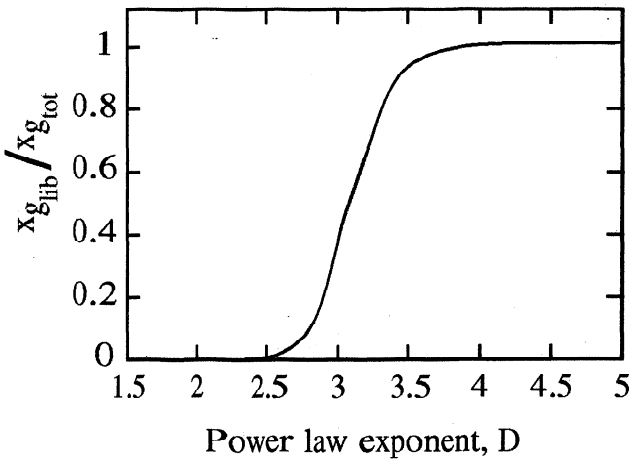

Figure 10. Fraction of gas released at fragmentation as a function of the D value of the size distribution of magma fragments. The fraction of gas is calculated as the ratio of the mass released ($x_{g_{\text{lib}}}$) to the total mass of gas exsolved from magma ($x_{g_{\text{tot}}}$). Note that it varies most dramatically when D is between 2.8 and 3.3.

5.2. Key Variables for Describing Pyroclast Populations

In pumices there is a large range of bubble sizes, and bubbles sizes may vary from eruption to eruption [*Cashman and Mangan*, 1994]. To evaluate the error involved, we have repeated the calculation of Figure 10 for two extreme values of the mean bubble size, 1 mm and 10 μm (Figure 11). Differences between these calculations are not negligible but are equivalent to changing the D value by 0.1, which is within the range of uncertainty. Polydispersed bubble populations can be treated using the method of Appendix B and do not change the results by more than 5% (Figure 12), which may be considered negligible.

To describe the gas/fragment mixture after fragmentation, one must therefore specify three parameters: the D value for the power law size distribution and the sizes of the smallest and largest fragments. If the power law exponent is smaller than 3, the population is controlled by large fragments and one might think that it is important to accurately determine the largest fragment size. This is not so because we are interested in the fraction of gas released. Whatever the largest fragment is, it is much larger than the average bubble size and hence contributes a negligible amount of continuous gas. On the other hand, if the power law exponent is larger than 3, the population is controlled by the small fragments. In this case, the smallest ash particles, with radii less 5 μm, say, are smaller than the majority of bubbles, and hence allow almost total gas release. It is therefore not important to specify accurately the smallest fragment size, as long as it is sufficiently small. Errors due to uncertainties in extreme fragment sizes do not exceed $\pm$ 5%. We therefore conclude that the main parameter

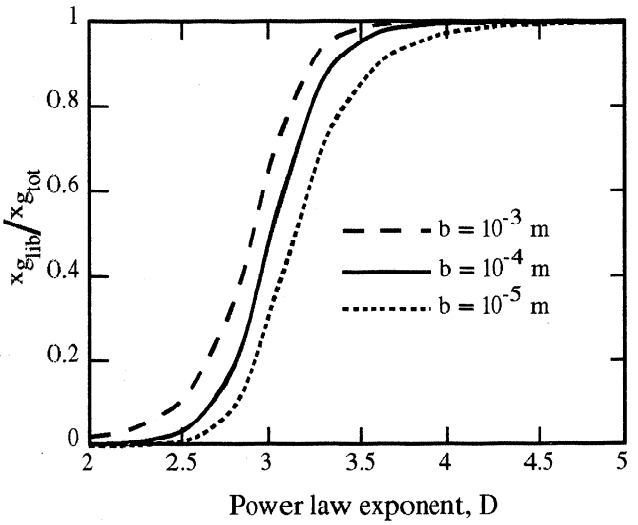

Figure 11. Fraction of gas released at fragmentation as a function of the D value of the size distribution of magma fragments, for three different values of the mean bubble size. The larger the bubble size, the smaller the fraction of gas which may be left within a fragment.

controlling the mass fraction of continuous gas is the exponent of the power law size distribution.

5.3. Flow Behaviour of the Gas/Fragment Mixture

At fragmentation, different flow regimes may ensue depending on the volume fraction of continuous gas in the gas/fragment mixture, noted α. Threshold values separating the different regimes depend somewhat on fragment shapes and size distributions [*Chong et al.*, 1971; *Chang and Powell*, 1993; *Ladd*, 1994], and the values quoted below must be considered approximate. For $\alpha \leq 0.25$ the fragments are almost packed. The mixture is not a suspension and its properties are essentially those of the fragments, that is, a viscous liquid. For intermediate values of α, between 0.25 and 0.75, the mixture behaves as a "slurry," with particle interactions playing a key role. Suspension behavior, such that fragments are freely suspended in the continuous gas phase and interact only via discrete collision events, is not achieved for $\alpha < 0.40$ [*de Kruif*, 1990]. For $\alpha \geq 0.75$, fragment interactions affect weakly flow behaviour and the mixture may be called "semidilute." Finally, for values of $\alpha \geq 0.95$, the dilute limit is reached, and the mixture may be described using the "dusty" gas approximation [*Marble*, 1970], such that its dynamic viscosity is equal to that for the pure gas phase.

In absolute values the quantity of gas released depends on the total amount which is exsolved when fragmentation occurs. Here, for consistency with previous studies, we fix the bulk volume fraction of gas available at fragmentation at the "conventional" value of 75% [*Woods*, 1995]. We note, however, that the following points would be much stronger were we to use the smaller value of 60% recently suggested by *Gardner et al.* [1996]. If the D value of the fragment population is larger than 3 at fragmentation, more than 60% of the gas present gets released, and α, the volume fraction of the continuous gas phase in the mixture, is larger than 45%. This makes the mixture a suspension, albeit a dense one. However, the experiments indicate that the D value at fragmentation is less than 3. In this case, less than 60% of the available gas gets released, and α is less than 45%. The mixture is not far from packing conditions such that most fragments touch one another. In this case, refragmentation is inevitable.

5.4. Secondary Fragmentation in a Volcanic Conduit

The experiments and theoretical considerations on fragmentation have explored situations which are much simpler than those of a true volcanic eruption. After "primary" fragmentation, the mass fraction of continuous gas increases due to refragmentation and gas expands because of decompression. In these conditions the flow characteristics tend towards "dilute" conditions, such that the collision probability drops to very small values. Two effects may contribute further increases of the volume fraction of continuous gas. Vesicular fragments may break up spontaneously due to bubble expansion. Bubble overpressures are not sensitive to fragment size [*Kaminski and Jaupart*, 1997], but one expects that small fragments with only a few bubbles do not fracture easily: a limit case is provided by a clast with only one bubble, for which bubble connection is

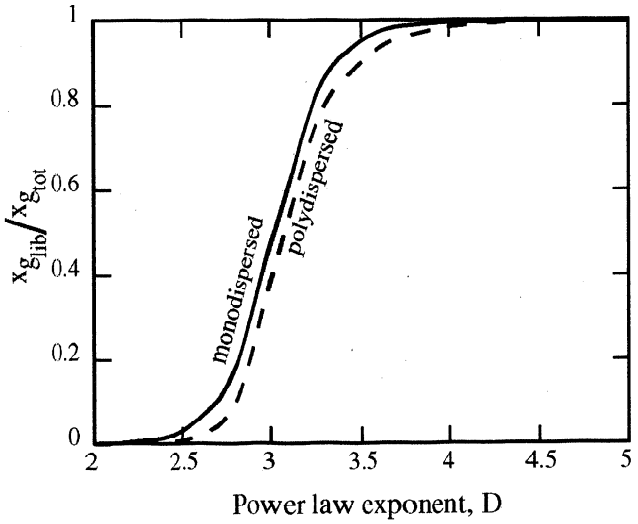

Figure 12. Fraction of gas released at fragmentation for two types of gas bubble populations. For an exact calculation, the smallest bubble size, the largest bubble size and the size distribution of fragments must be specified. In the "monodispersed" population, all bubbles have the same size. The "polydispersed" bubble population is described by a power law (Appendix B) and has the same mean bubble size.

obviously impossible. Thus this process is likely to increase the proportion of fines in the fragment population. However, it is hard to see how it may account for the size distribution of the fine fraction, which has the same D value than the coarse fraction. Additionally, some vesicular fragments may be permeable and leak some of their gas to the continuous phase. We argue in Appendix A that both effects are not important in a volcanic conduit.

6. Discussion

6.1. Characteristics of Pyroclastic Populations

The pyroclastic deposits studied in this paper have three outstanding characteristics which may be summarized simply using their D values. First, there is no single D value for all the deposits. This may seem surprising because, in all the industrial and natural fragment populations referenced by *Turcotte* [1986], a given fragmentation mechanism acting on given material is associated with a single and specific value of the exponent. However, we know that exponents larger than 3 cannot be due to a single "primary" fragmentation event and that they can be produced by selective refragmentation. We therefore imagine fragments continuously colliding and fragmenting in the volcanic flow, with the size distribution continuously evolving. Because of expansion, the power law exponent gets "frozen" at various values smaller than the steady-state limit. Another way of stating this is that a large range of D values and values larger than 3 are two symptoms of the same refragmentation sequence. Second, it is remarkable that the histogram of D values for fall deposits has a sharp cutoff at the value of 3.0 (Figure 7). With exponent values smaller than 3.0, the amount of gas released at fragmentation is a small fraction of the total available (Figure 10), and such conditions are not in favor of a sustained Plinian regime which requires a minimum amount of continuous gas [*Woods*, 1995]. A rigorous test requires a calculation involving the mass discharge rate and the initial amount of volatiles present in the melt, and must be done for specific case histories. For space reasons, this is developed in a companion paper. Third, histograms for the pyroclastic flow and fall deposits are not identical (Figure 7), and the flow exponents are systematically smaller than their fall counterparts. This is consistent with fluid dynamical considerations, as it is now well established that, all else being equal, pyroclastic flows are generated for smaller gas contents than Plinian columns. Finally, we note that, amongst the 62 deposits studied, the smallest exponent value is 2.9 (Tables 1-3), which is larger than the experimental values for "primary" fragmentation.

We conclude that the systematics of D values for the 62 deposits studied are consistent with basic physical constraints. Further, these systematics indicate that D is a key variable for the dynamics of eruption.

6.2. Fragmentation Sequence in Explosive Volcanic Eruptions

Using the above results, we may build a qualitative model for the ascent of magma in an eruption conduit involving three stages (Figure 13). The first stage is "primary" fragmentation, such that $D \approx 2.6$: this marks the transition from magmatic foam to dense granular mixture. For such small D values the continuous gas phase amounts to about 20% of the total volume of gas present, and α, the volume fraction of continuous gas in the mixture, is only about 15%. The fragments are therefore near packing conditions. The second stage is a rheological transition, such that the mixture becomes a suspension, which occurs when α is larger than about 40%. At constant D value, and hence for a constant mass fraction of continuous gas in the mixture, this requires a large amount of expansion. For an ideal gas and isothermal decompression, pressure must decrease by a factor of 5 to go from $\alpha = 15\%$ to $\alpha = 45\%$. During this decompression, however, refragmentation occurs and induces an increase of the D value. The transition to suspension behavior may therefore be defined in a more appropriate manner by a threshold value for D, and we propose $D \approx 3.0$. The third stage is when the fragment population stops evolving, which may be reached before ejection into the atmosphere. It is only at this stage that the mass fraction of continuous gas in the mixture is set. In this framework, therefore, the conditions for a Plinian plume or a pyroclastic flow may in fact be established by refragmentation in the volcanic conduit.

The above considerations on refragmentation introduce time as a key variable and emphasize the different effects of collision and decompression on the fragment size distribution. The collision rate depends on the local turbulence of the flow, which is related to the mean vertical velocity. The decompression rate depends on vertical velocity, which increases as the amount of continuous gas increases. The flow conditions and the size distribution of fragments are therefore coupled. If the decompression rate is large, expansion may limit the extent of refragmentation and the D value may not increase rapidly. In this case, the mixture of gas and fragments erupting out the vent may have relatively small D values and hence may not be dilute. The fact that some pyroclastic flow deposits have D values of 3.0 or less must be taken into account when debating whether these flows were dilute or dense.

7. Conclusion

The grain size distributions of Plinian and pyroclastic flow deposits follow power laws as do many other fragment populations. Plinian populations stand out because they all have power law exponents larger than 3. Such large values are explained by selective refragmentation due to fragment collisions. During flow and de-

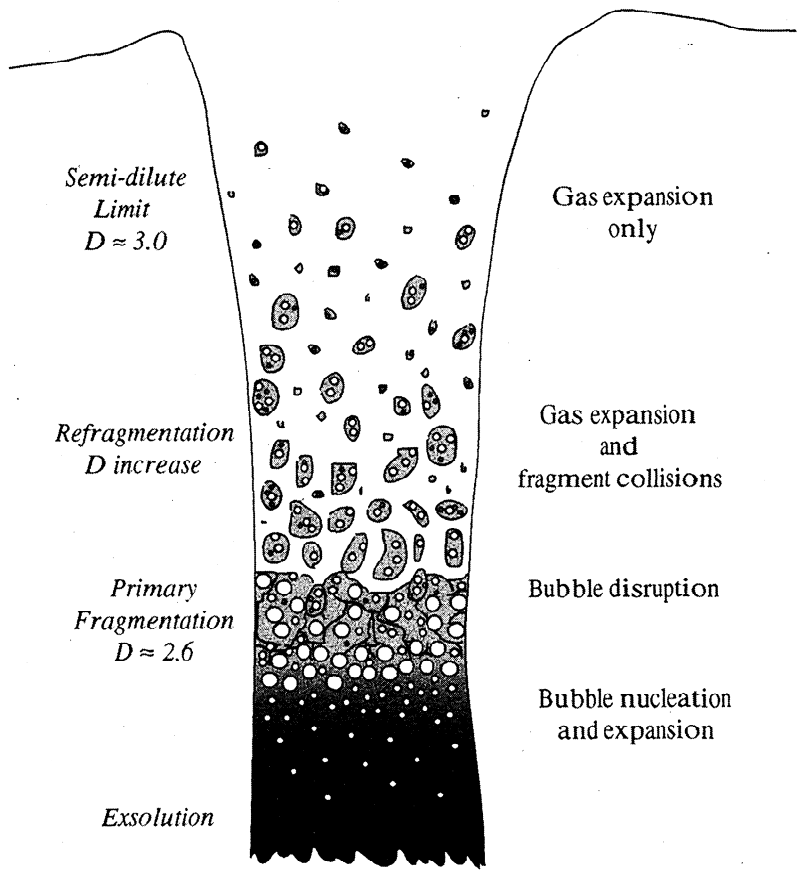

Figure 13. Schematic representation of three important levels in the fragmentation sequence of an explosive volcanic eruption.

compression in a volcanic conduit, the power law exponent of the fragment population continuously increases from an initial value of about 2.5±0.1. One must therefore speak of a "fragmentation sequence" instead of a single fragmentation event. In the volcanic mixture, the amount of continuous gas which carries fragments in suspension is very sensitive to the power law exponent of the size distribution. Thus in order to predict eruptive behavior above the vent, it is not sufficient to determine which fragmentation mechanism operates in the volcanic conduit. One must also specify which size distribution is generated and how it evolves during ascent towards Earth's surface.

Appendix A: Permeability of Pumice Samples

Gas bubbles within a fragment may be connected to the exterior, in which case they contribute gas to the "continuous" phase. Pumice samples are usually permeable when found in a deposit. This may be due to cooling and quenching, which lead to the rupture of the thin magma films encasing bubbles [*Mungall et al.*, 1996]. This may have been achieved earlier, however, and one must assess when. This has been attempted using textural observations [*Klug and Cashman*, 1996], determinations of the extent of oxydation reactions within the matrix glass [*Tait et al.*, 1998], and theoretical calculations of fragment evolution together with systematic investigations of pumice vesicularity [*Gardner et al.*, 1996; *Kaminski and Jaupart*, 1997].

One may argue that highly vesicular samples are not stable and become permeable as soon as vesicularity reaches a critical value of about 70%. This is not so for all pumices, as shown by the occurrence of "reticulites" with vesicularities of up to 97% [*Cashman and Mangan*, 1994]. Such extreme samples are commonly produced by basaltic fire fountains and have been dismissed as unrepresentative of Plinian conditions. However, they have also been found in Plinian deposits from phonolitic eruptions involving magmas of intermediate viscosity [*Gardner et al.*, 1996]. Such samples demonstrate that, in turbulent volcanic flows, vesicular fragments can expand to extremely large vesicularity values without damage.

Inside pumice fragments, *Klug and Cashman* [1996] found many interrupted vesicle walls with rounded edges and contorted shapes, suggesting that permeability developed whilst magma was still liquid. Unfortunately, this does not constrain the timing of bubble connection

as the interior of vesicular fragments remains hot for times which are large compared to the times for eruption and expansion in the atmospheric column [*Kaminski and Jaupart*, 1997]. Such internal textural features are difficult to interpret in terms of bulk permeability because of the large gradients of stress and temperature which are set up in vesicular fragments [*Kaminski and Jaupart*, 1997]. Bubble connection to the exterior is made difficult by the presence of a dense outer shell at the edge of pumices, where vesicularity is smaller than in the interior [*Gardner et al.*, 1996].

For typical magma compositions and eruption conditions, one should expect pumice vesicularity to reach values larger than 95%, and this is indeed achieved in reticulites. Most pumices have lower vesicularity values, and the conventional explanation has been early bubble connection [e.g., *Sparks*, 1978]. However, an alternative mechanism is quenching during expansion in the atmospheric eruption column [*Thomas et al.*, 1994]. Quenching initially affects a thin rind at the edge of fragments, but this is sufficient to halt expansion of the whole fragment. Bubble connection and quenching are not mutually exclusive and one must determine their relative importances for the fragment population as a whole. Bubble connection is an intrinsically probabilistic phenomenon, and the answer must first involve a quantitative analysis of expansion and quenching without permeability development. This has been carried out by *Kaminski and Jaupart* [1997], who were able to explain the bulk characteristics of many Plinian fall deposits. Their analysis does not account for a small number of samples in these deposits, which have low values of vesicularity. The conclusion is that the vast majority of magma fragments become permeable late in the eruption sequence, after cooling and quenching in the atmospheric column, and hence after ejection into the atmosphere. This implies that the "dispersed" gas phase remains essentially trapped within fragments in the volcanic conduit.

Appendix B: Amount of Gas Released at Fragmentation

B1. Monodisperse Bubble Population

Just after fragmentation, bubbles which have been intersected by the fragmentation surface leave part of their walls, and the outer edge of fragments is rough and jagged. The fragment volume includes these protuberances. Because of surface tension, some of these pointed bits may retract [*Gardner et al.*, 1996]. We neglect this and introduce two new variables: $\bar{S}_b$, the average cross section of a bubble at the fragment surface, and $\bar{V}_b$, the average volume of gas of an intersected bubble below the fragmentation surface (Figure 14).

If N_b^* is the number of bubbles disrupted by fragmentation in a single clast, the volume of gas released by N_f clasts is equal to

$$V_{\text{out}} = N_f N_b^* \bar{V}_b. \tag{B1}$$

We consider that bubbles are randomly distributed in a fragment and initially assume that the fragment is much larger than the bubbles. A straightforward calculation shows that the curvature of the fragment surface can be neglected. If the volume fraction of gas within the bubbly magma is ϵ, the surface fraction of gas on an arbitrary plane cutting through the volume is also ϵ [*Underwood*, 1970, p. 23]. This theorem is valid for a large surface where many bubbles may be found and does not apply to a small fragment. Here, however, we are dealing with a large population of fragments, and hence with a large cumulative area. For a single fragment, the mean surface available for bubbles is

$$S_{\text{gas}} = \epsilon 4\pi r^2 = N_b^* \bar{S}_b. \tag{B2}$$

From this equation the number of intersected bubbles is given by

$$N_b^* = \epsilon 4\pi \frac{r^2}{\bar{S}_b}. \tag{B3}$$

Collecting terms, we find

$$\frac{V_{\text{out}}}{V_{\text{gas}}} = \frac{\epsilon N_f 4\pi \frac{r^2}{\bar{S}_b} \bar{V}_b}{\epsilon N_f \frac{4}{3}\pi r^3} = \frac{3}{r}\frac{\bar{V}_b}{\bar{S}_b}. \tag{B4}$$

Bubbles with radius b can be intersected at various levels. We call h the distance between the lowest point in the bubble and the cutting plane (Figure 14), which may vary from 0 to 2 b. $S(h)$ is the area occupied by a bubble at the fragment surface, equal to

$$S(h) = \pi \left(2bh - h^2\right). \tag{B5}$$

The associated volume of gas which lies below the cutting plane is

$$V(h) = \frac{\pi}{3} h^2 \left(3b - h\right). \tag{B6}$$

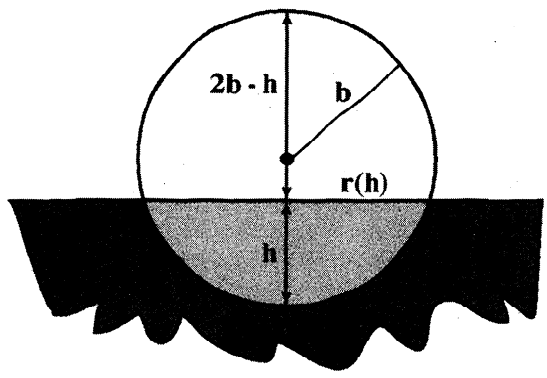

Figure 14. Sketch of a bubble near the surface of a fragment. The bubble radius is b. The volume of gas in the spherical cap of depth h is released by fragmentation and collects into a continuous gas phase.

The mean intersected area is thus

$$\bar{S}_b = \frac{1}{2b}\int_0^{2b} S(h)dh = \frac{2}{3}\pi b^2. \quad \text{(B7)}$$

Similarly, the average volume of gas available below the cutting plane is found to be

$$\bar{V}_b = \frac{1}{2b}\int_0^{2b} V(h)dh = \frac{2}{3}\pi b^3. \quad \text{(B8)}$$

Substituting for the various expressions in (B4), we find

$$\frac{V_{\text{out}}}{V_{\text{gas}}} = \frac{3b}{r}, \quad \text{(B9)}$$

which is half the upper bound derived in the main text (equation (6)). This equation is obviously not valid for fragments with radii smaller than $3\,b$, and one must use a different analysis.

For a fragment which is not large compared to its bubbles, the fraction of gas released depends on the exact shape of the fragment and on the packing arrangement of bubbles. The surface of the fragment has significant curvature and may not be locally approximated by a plane. An accurate calculation would require elaborate geometrical considerations but would not be really useful for our purposes. We first estimate the smallest fragment size such that (B9) applies, that is, such that large number statistics apply. Pumices have been extensively sampled down to a size of 0.8 cm. These have

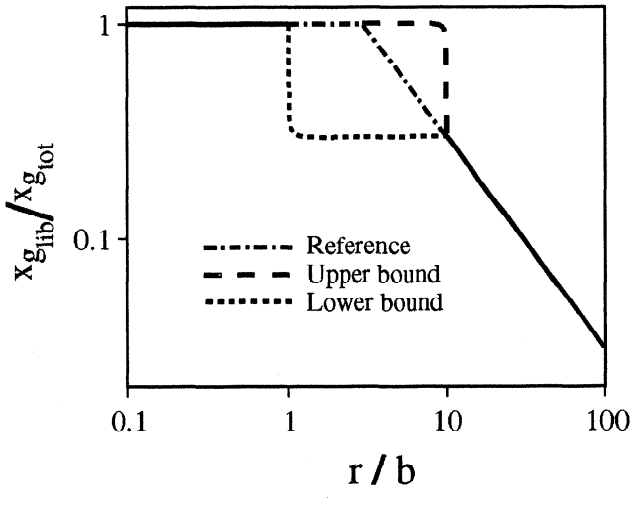

Figure 15. Fraction of gas released by an individual fragment as a function of size r normalized to the bubble radius b. The fraction of gas is calculated as the ratio of the mass released ($x_{g_{\text{lib}}}$) to the total mass of gas exsolved ($x_{g_{\text{tot}}}$). Three different approximations are used for fragments which cannot be considered large compared to gas bubbles, that is, such that $r/b \leq 10$. The upper bound is such that these fragments release all their gas. The lower bound corresponds to the other extreme: these fragments release a fixed amount of gas set equal to the value for $r/b = 10$.

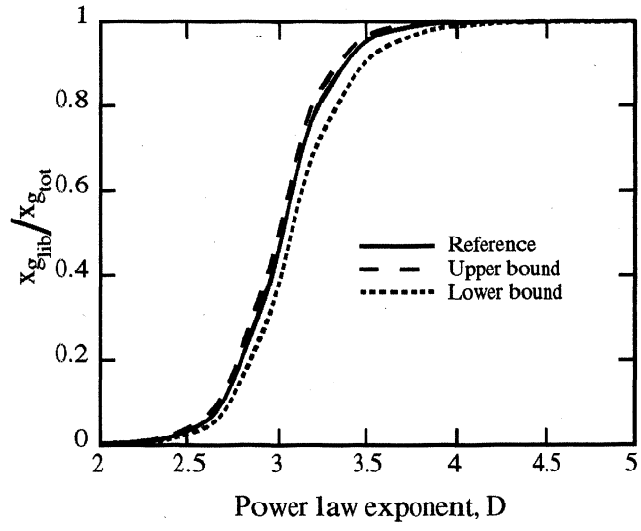

Figure 16. Fraction of gas released at fragmentation as function of the power law exponent D of the fragment size distribution for the three cases of Figure 15. Bubble radius b is taken to be 10^{-4} m.

vesicularities and shapes which do not depend on size [*Houghton and Wilson*, 1989; *Gardner et al.*, 1996]. Using $b = 10^{-4}$ m, which is a typical average bubble size, such fragments are at least 100 times larger than the average bubble and can indeed be considered large compared to the bubbles. We may extend this to fragment sizes as small as 10 x b because the fragment/bubble volume and surface ratios still take large values. We know that a fragment which is smaller than a bubble cannot retain any gas, and hence what is required is an estimation procedure for small fragments with sizes in the range from b to 10 x b. We use the fact that the fraction of gas kept within a fragment decreases as the fragment size gets smaller and calculate upper and lower bounds (Figure 15). For the upper bound we assume that fragments with radii less than 10 x b release all their gas. For a lower bound we take the amount of gas released by fragments with radii between 10 x b and b to be equal to the amount for r = 10 x b. We find that these two bounds differ by less than 5% (Figure 16), which is negligible. For reference, calculations will be carried out for an intermediate model, using (B9) down to r = 3 x b and assuming that all the gas gets released for $r \leq 3$ x b (Figure 15). The accuracy of this "reference" calculation is sufficient for our purposes (Figure 16).

B2. Polydispersed Bubble Population

Consider a bubble with given radius b which extends to depth h into a fragment. Variable h may vary from 0 to a maximum value $h_{\max}$. If the bubble is smaller than the fragment, $h_{\max} = 2b$ and hence quantities $\bar{S}_b$ and $\bar{V}_b$ are as above. If the bubble is larger than the fragment, $h_{\max} = r$ and

$$\bar{S}_b = \pi\left(br - \frac{r^2}{3}\right), \quad \text{(B10)}$$

$$\bar{V}_b = \frac{\pi}{3}\left(br^2 - \frac{r^3}{4}\right). \quad \text{(B11)}$$

In a bubble population with sizes ranging from a minimum value $b_{\min}$ to a maximum value $b_{\max}$, the fraction of bubbles with radius between b and $b + db$ is called dN_b. The total area occupied by bubbles at the fragment surface is

$$4\pi\epsilon r^2 = \int_{b_{\min}}^{b_{\max}} S_b\, dN_b, \quad \text{(B12)}$$

and the volume of gas trapped inside the fragment is

$$V_{\text{int}}(r) = \frac{4}{3}\pi r^3\epsilon - \int_{b_{\min}}^{b_{\max}} V_b\, dN_b. \quad \text{(B13)}$$

We consider that the bubble population also follows a power law distribution with an exponent B between 2 and 3 [*Gaonac'h et al.*, 1996]. Accordingly, the number of bubbles with radii a larger than b is

$$N_b(a \geq b) = \beta b^{-B}, \quad \text{(B14)}$$

where β is a renormalization coefficient which must be solved for. The area occupied by bubbles at the surface of a fragment is equal to

$$4\pi\epsilon r^2 = \beta \int_{b_{\min}}^{r/2} (-B) b^{-B-1} \tfrac{2}{3}\pi b^2 db + \beta \int_{r/2}^{b_{\max}} (-B) b^{-B-1} \pi\left(br - \tfrac{r^2}{3}\right) db, \quad \text{(B15)}$$

from which we can extract β to evaluate the volume of bubbles inside the fragment, $V_{\text{int}}(r)$. Finally, the total volume of gas preserved in a fragment population characterized by a power law size distribution (13) is

$$V_{\text{in}} = \int_{r_{\min}}^{r_{\max}} V_{\text{int}}(r)\lambda(-D) r^{-D-1} dr. \quad \text{(B16)}$$

The amount of gas which gets released is calculated using the total volume of gas present

$$V_{\text{out}} = \epsilon\frac{4}{3}\pi \int_{r_{\min}}^{r_{\max}} \lambda(-D) r^{-D-1} r^3 dr - V_{\text{in}}. \quad \text{(B17)}$$

We take $B = 2.7$, $b_{\min} = 2.5$ μm and $b_{\max}$=2.5 mm (Figure 12). There is only a small difference with a monodisperse bubble population with the same average bubble size.

Acknowledgments. We thank Stephen Sparks and Lionel Wilson for their suggestions and, as usual, for their positive and helpful discussions. The manuscript was improved by the comments of the Associate Editor. Funding was provided by the Programme National d'Étude des Risques Naturels, CNRS - INSU, France.

References

Alibidirov, M., and D. B. Dingwell, Magma fragmentation by rapid decompression, *Nature, 380*, 146–148, 1996.

Allègre, C. J., J. L. Le Mouel, and A. Provost, Scaling rules in rock fracture and possible implications for earthquake prediction, *Nature, 297*, 47–49, 1982.

Anderson, A. T., S. Newman, S. N. Williams, T. H. Druitt, C. Skirius, and E. Stolper, H_2O, CO_2, Cl, and gas in plinian and ash-flow Bishop rhyolite, *Geology, 17*, 221–225, 1989.

Anilkumar, A. V., R. S. J. Sparks, and B. Sturtevant, Geological implications and applications of high-velocity two-phase flow experiments, *J. Volcanol. Geotherm. Res., 56*, 145–160, 1993.

Bloomfield, K., G. Sanchez Rubio, and L. Wilson, Plinian eruptions of Nevado de Toluca volcano, Mexico, *Geol. Rundsch., 66*, 120–145, 1977.

Booth, B., The Granadilla pumice deposit of southern Tenerife, Canary islands, *Proc. Geol. Assoc., 84*, 353–370, 1973.

Boudon, G., G. Camus, P. Gourgaud, and J. Lajoie, The 1984 nuée ardente deposits of Merapi volcano, Central Java, Indonesia: Stratigraphy, textural characteristics and transport mechanisms, *Bull. Volcanol., 55*, 327–342, 1993.

Braitseva, O. A., I. V. Melekestsev, V. V. Ponomareva, and V. Y. Kirianov, The caldera-forming eruption of Ksudach volcano about cal. AD 240: The greatest explosive event of our era in Kamchatka, Russia, *J. Volcanol. Geotherm. Res., 70*, 49–65, 1996.

Brazier, S., A. N. Davis, H. Sigurdsson, and R. S. J. Sparks, Fall-out and deposition of volcanic ash during the 1979 explosive eruption of the Soufrière of Saint Vincent, *J. Volcanol. Geotherm. Res., 14*, 335–359, 1982.

Bursik, M. I., R. S. J. Sparks, J. S. Gilbert, and S. N. Carey, Sedimentation of tephra by volcanic plumes, I, Theory and its comparison with a study of Fogo A plinian deposit, Sao Miguel (Azores), *Bull. Volcanol., 54*, 329–344, 1992.

Carey, S., and H. Sigurdsson, Influence of particle aggregation on deposition of distal tephra from May 1980 eruption of Mount St. Helens volcano, *J. Geophys. Res., 87*, 7061–7072, 1982.

Carey, S., H. Sigurdsson, J.E. Gardner and W. Criswell, Variations in column height and magma discharge during the May 18, 1980 eruption of Mount St. Helens, *J. Volcanol. Geotherm. Res., 43*, 99–112, 1990.

Carey, S., H. Sigurdsson, C. Mandeville, and S. Bronto, Pyroclastic flows and surges over water: An example from the 1883 Krakatau eruption, *Bull. Volcanol., 57*, 493–511, 1996.

Cargill, S. M., D. H. Root, and E. H. Bailey, Estimating usable resources from historical industry data, *Econ. Geol., 76*, 1081–1095, 1981.

Cashman, K. V., and M. T. Mangan, Physical aspects of magmatic degassing, II, Constraints on vesiculation processes from textural studies of eruptive products, in *Volatiles in Magmas*, edited by M.R. Carroll and J.R. Holloway, *Rev. Mineral., 30*, 447-478, 1994.

Chang, C., and R. L. Powell, Dynamic simulation of bimodal suspensions of hydrodynamically interacting spherical particles, *J. Fluid Mech., 253*, 1–25, 1993.

Cheng, Z., and S. Redner, Kinetics of fragmentation, *J. Phys. A. Math. Gen., 23*, 1233–1258, 1990.

Chong, J. S., E. B. Christiansen, and A. D. Baer, Rheology of concentrated suspensions, *J. Appl. Polym. Sci., 15*, 2007–2021, 1971.

de Kruif, C. G., The rheology of colloidal dispersions in relation to their microstructure, in *Hydrodynamics of Dis-*

persed Media, edited by J. P. Hulin, A. M. Cazabat, E. Guyon, and F. Carmona, pp. 79–101, Elsevier Sci., New York, 1990.

Dellino, P., and L. La Volpe, Fragmentation versus transportation mechanisms in the pyroclastic sequence of Monte Pilato-Rocche Rosse (Lipari, Italy), *J. Volcanol. Geotherm. Res., 64*, 211–231, 1995.

Dombrowski, N., and W. R. Johns, The aerodynamic instability and disintegration of viscous liquid sheets, *Chem. Eng. Sci., 18*, 203–214, 1963.

Fisher, R. V., Maximum size, median diameter, and sorting of tephra, *J. Geophys. Res., 69*, 341–355, 1964.

Fisher, R.V., and H.-U. Schmincke, *Pyroclastic Rocks*, 472 pp., Springer Verlag, New York, 1984.

Gardner, J. E., R. M. E. Thomas, C. Jaupart, and S. Tait, Fragmentation of magma during Plinian volcanic eruptions, *Bull. Volcanol., 58*, 144–162, 1996.

Gaonac'h, H., J. Stix, and S. Lovejoy, Scaling effects on vesicle shape, size and heterogeneity of lavas from Mount Etna, *J. Volcanol. Geotherm. Res., 74*, 131–153, 1996.

Hartmann, W. K., Terrestrial, lunar and interplanetary rock fragmentation, *Icarus, 10*, 201–213, 1969.

Hayakawa, Y., Pyroclastic geology of Towada volcano, *Bull. Earthquake Res. Inst. Univ. Tokyo, 60*, 507–592, 1985.

Hinze, J. O., Fundamentals of the hydrodynamic mechanism of splitting in dispersion processes, *AIChE J., 1*, 289–295, 1955.

Houghton, B. F., and C. J. N. Wilson, A vesicularity index for pyroclastic deposits, *Bull. Volcanol., 51*, 451–462, 1989.

Kaminski, É., and C. Jaupart, Expansion and quenching of vesicular magma fragments in Plinian eruptions, *J. Geophys. Res., 102*, 12,187–12,203, 1997.

Katsui, Y., On the Shikotsu Pumice-fall deposit, special reference to the activity just before the depression of the Shikotsu caldera, *Bull. Volcanol. Soc. Jpn., 4*, 33-48, 1959.

Klug, C., and K. V. Cashman, Vesiculation of May 18, 1980, Mount St. Helens magma, *Geology, 22*, 468–472, 1994.

Klug, C., and K. V. Cashman, Permeability development in vesiculating magmas: Implications for fragmentation, *Bull. Volcanol., 58*, 87–100, 1996.

Koyaguchi, T., Grain-sized variation of tephra derived from volcanic umbrella clouds, *Bull. Volcanol., 56*, 1–9, 1994.

Ladd, A. J. C., Numerical simulations of particulate suspensions via a discretized Boltzmann equation, 2, Numerical results, *J. Fluid Mech., 271*, 311–339, 1994.

Lyakhovsky, V., S. Hurwitz, and O. Navon, Bubble growth in rhyolitic melts: Experimental and numerical investigation, *Bull. Volcanol., 58*, 19–32, 1996.

Macedonio, G., F. Dobran, and A. Neri, Erosion processes in volcanic conduits and an application to the AD79 eruption of Vesuvius, *Earth Planet. Sci. Lett., 121*, 267–280, 1994.

Mader, H. M., Y. Zhang, J. C. Phillips, R. S. J. Sparks, B. Sturtevant, and E. Stolper, Experimental simulations of explosive degassing of magma, *Nature, 372*, 85–88, 1994.

Marble, F. E., Dynamics of dusty gases, *Annu. Rev. Fluid Mech., 2*, 397–446, 1970.

Mungall, J. E., N. S. Bagdassarov, C. Romano, and D. B. Dingwell, Numerical modelling of stress generation and microfracturing of vesicle walls in glassy rocks, *J. Volcanol. Geotherm. Res., 73*, 33–46, 1996.

Murai, I., A study of the textural characteristics of pyroclastic flow deposits in Japan, *Bull. Earthquake Res. Inst. Univ. Tokyo, 39*, 133–248, 1961.

Nairn, I. A., and S. Self, Explosive eruptions and pyroclastic avalanches from Ngauruhoe in February 1975, *J. Volcanol. Geotherm. Res., 3*, 39–60, 1978.

Neri, A., and G. Macedonio, Numerical simulation of collapsing volcanoc columns with particles of two sizes, *J. Geophys. Res., 101*, 8153–8174, 1996.

Phillips, J. C., S. J. Lane, A.-M. Lejeune, and M. Hilton, Gum rosin-acetone system as an analogue to the degassing behaviour of hydrated magmas, *Bull. Volcanol., 57*, 263–268, 1995.

Proussevich, A. A., D. L. Sahagian, and A. T. Anderson, Dynamics of diffusive bubble growth in magmas: Isothermal case, *J. Geophys. Res., 98*, 22,283–22,308, 1993.

Pyle, D. M., The thickness, volume and grain size of tephra fall deposits, *Bull. Volcanol., 51*, 1–15, 1989.

Ranz, W. E., On sprays and spraying, *Eng. Res. Bull., B-65*, 75 pp., Pa. State Univ., University Park, 1959.

Redner, S., Fragmentation, in *Random Material and Processes, Statistical Models for the Fracture of Disordered Media*, edited by H. J. Herrmann and S. Roux, pp. 321–348, North-Holland, New York, 1990.

Reitz, R. D., and F. V. Bracco, Mechanism of atomisation of a liquid jet, *Phys. Fluids, 25*, 1730–1742, 1982.

Rutherford, M. J., H. Sigurdsson, S. Carey, and A. Davis, The May 18, 1980, eruption of Mount St. Helens, 1, Melt composition and experimental phase equilibria, *J. Geophys. Res., 90*, 2929–2947, 1985.

Scasso, R. A., H. Corbella, and P. Tiberi, Sedimentological analysis of the tephra from the 12–15 August 1991 eruption of Hudson volcano, *J. Volcanol. Geotherm. Res., 56*, 121–132, 1994.

Self, S., Large-scale phreatomagmatic silicic volcanism: A case study from New Zealand, in *Explosive Volcanism*, edited by M. F. Sheridan and F. Barberi, *J. Volcanol. Geotherm. Res., 17*, 433–469, 1983.

Silverman, I., and W. A. Sirignano, Multi-droplet interaction effects in dense sprays, *Int. J. Multiphase Flow, 20*, 99–116, 1994.

Sparks, R. S. J., The dynamics of bubble formation and growth in magmas: A review and analysis, *J. Volcanol. Geotherm. Res., 3*, 1–37, 1978.

Sparks, R. S. J., and G. P. L. Walker, The significance of vitric-enriched air-fall ashes associated with crystal-enriched ignimbrites, *J. Volcanol. Geotherm. Res., 2*, 329–341, 1977.

Sparks, R. S. J., and L. Wilson, A model for the formation of ignimbrite by gravitational column collapse, *J. Geol. Soc. London, 132*, 441–451, 1976.

Sparks, R. S. J., L. Wilson, and H. Sigurdsson, The pyroclastic deposits of the 1875 eruption of Askja, Iceland, *Philos. Trans. R. Soc. London Ser. A, 299*, 241–273, 1981.

Sparks, R. S. J., J. Barclay, C. Jaupart, H. M. Mader, and J. C. Phillips, Physical aspects of magmatic degassing, I, Experimental and theoretical constraints on vesiculation, in *Volatiles in Magmas*, edited by M. R. Carroll and J. R. Holloway, *Rev. Mineral., 30*, 413–445, 1994.

Sugioka, I., and M. Bursik, Explosive fragmentation of erupting magma, *Nature, 373*, 689–692, 1995.

Suzuki, T., Y. Katsui, and T. Nakamura, Size distribution of the Tarumai Ta-b pumice fall deposit. *Bull. Volcanol. Soc. Jpn., 18*, 47–64, 1973.

Tait, S., R. Thomas, J. Gardner, and C. Jaupart, Constraints on cooling rates and permeabilities of pumice in an explosive eruption jet from colour and magnetic mineralogy, *J. Volcanol. Geotherm. Res.*, in press, 1998.

Thomas, N., C. Jaupart, and S. Vergniolle, On the vesicularity of pumice, *J. Geophys. Res., 99*, 15,633–15,644, 1994.

Turcotte, D. L., Fractals and fragmentation, *J. Geophys. Res., 91*, 1921–1926, 1986.

Turcotte, D.L., *Fractals and Chaos in Geology and Geophysics*, 221 pp., Cambridge Univ. Press, New York, 1992.

Underwood, E. E., *Quantitative Stereology*, 274 pp., Addison-Wesley, Reading, Mass., 1970.

Valentine, G., and K. Wohletz, Numerical models of Plinian eruption columns, *J. Geophys. Res., 94*, 1867–1887, 1989.

Walker, G. P. L., Grain-size characteristics of pyroclastic deposits, *J. Geol., 79*, 696–714, 1971.

Walker, G. P. L., Explosive volcanic eruptions: A new classification scheme, *Geol. Rundsch., 62*, 431–446, 1973.

Walker, G. P. L., The Taupo pumice: Product of the most powerful known (Ultraplinian) eruption?, *J. Volcanol. Geotherm. Res., 8*, 69–94, 1980.

Walker, G. P. L., The Waimihia and Hatepe plinian deposits from rhyolitic Taupo Volcanic Centre. *N.Z. J. Geol. Geophys., 24*, 305–324, 1981a.

Walker, G. P. L., Plinian eruptions and their products, *Bull. Volcanol., 44-2*, 223–240, 1981b.

Walker, G. P. L., and R. Croasdale, Two plinian- type eruptions in the Azores, *J. Geol. Soc. London, 127*, 17–55, 1970.

Walker, G. P. L., and C. J. N. Wilson, Lateral variations in the Taupo ignimbrite, *J. Volcanol. Geotherm. Res., 18*, 117–133, 1983.

Wiesner, M. G., Y. Wang, and L. Zheng, Fallout of volcanic ash to the deep South China Sea induced by the 1991 eruption of Mount Pinatubo (Philippines), *Geology, 23*, 885–888, 1995.

Williams, S. N., and S. Self, The October 1902, plinian eruption of Santa Maria Volcano, Guatemala, *J. Volcanol. Geotherm. Res., 16*, 33–56, 1983.

Wilson, L., Explosive volcanic eruptions, III, Plinian eruption columns, *Geophys. J. R. Astron. Soc., 45*, 543–556, 1976.

Wilson, L., R. S. J. Sparks, and G. P. L. Walker, Explosive volcanic eruption, IV, The control of magma properties and conduit geometry on eruption column behaviour, *Geophys. J. R. Astron. Soc., 63*, 651–679, 1980.

Wohletz, K. H., Mechanisms of hydrovolcanic pyroclast formation: Grain-size, scanning electron microscopy, and experimental studies, *J. Volcanol. Geotherm. Res., 17*, 31–64, 1983.

Wohletz, K. H., M. F. Sheridan, and W. K. Brown, Particle size distributions and sequential fragmentation/transport theory applied to volcanic ash, *J. Geophys. Res., 94*, 15,703–15,721, 1989.

Woods, A. W., The dynamics of explosive volcanic eruptions, *Rev. Geophys., 33*, 495–530, 1995.

Woods, A. W., and M. I. Bursik, Particle fallout, thermal disequilibrium and volcanic plumes, *Bull. Volcanol., 53*, 559–570, 1991.

Wright, J. V., and G. P. L. Walker, Eruption, transport and deposition of ignimbrite: A case study from Mexico, *J. Volcanol. Geotherm. Res., 9*, 111–131, 1981.

C. Jaupart and É. Kaminski, Institut de Physique du Globe, 4. Pl. Jussieu, F-75252, Paris cedex 5, France. (e-mail: cj@ccr.jussieu.fr; kaminski@ipgp.jussieu.fr)

(Received February 18, 1998; revised July 21, 1998; accepted August 19, 1998.)